TOPICAL REVIEW

Quantum effects in electrical and thermal transport through nanowires

View the article online for updates and enhancements.

Related content

- An atomistic study on the stretching of nanowires
  H Mehrez, S Ciraci, C Y Fong et al.

- Quantum heat transfer through an atomic wire
  A Buldum, S Ciraci and C Y Fong

- Physics of carbon nanotube electronic devices
  M P Anantram and F Léonard

Recent citations

- On prototypical wave transmission across a junction of waveguides with honeycomb structure
  Basant Lal Sharma

- Analytical modeling of the lattice and thermo-elastic coefficient mismatch-induced stress into silicon nanowires horizontally embedded on insulator-on-silicon substrates
  Sulagna Chatterjee and Sanatan Chattopadhyay

- Theoretical Investigation of Relationship between Quantum Chemical Descriptors, Topological Indices, Energy and Electric Moments of Zig-zag Polyhex Carbon Nanotubes TUHC6 [2p,q] with Various Circumference [2p] and Fixed Lengths
  Mohammad Goodarzi and Esmat Mohammadinasab

IOP ebooks™

Bringing you innovative digital publishing with leading voices to create your essential collection of books in STEM research.

Start exploring the collection - download the first chapter of every title for free.

TOPICAL REVIEW

Quantum effects in electrical and thermal transport through nanowires

S Ciraci[1,2,4]**, A Buldum**[3] **and Inder P Batra**[1]

[1] Department of Physics, University of Illinois at Chicago, Chicago, IL 60607-7059, USA
[2] Department of Physics, Bilkent University, Bilkent, Ankara 06533, Turkey
[3] Department of Physics and Astronomy, The University of North Carolina at Chapel Hill, Chapel Hill, NC 27599, USA

Abstract
Nanowires, point contacts and metallic single-wall carbon nanotubes are one-dimensional nanostructures which display important size-dependent quantum effects. Quantization due to the transverse confinement and resultant finite level spacing of electronic and phononic states are responsible for some novel effects. Many studies have revealed fundamental and technologically important properties, which are being explored for fabricating future nanodevices. Various simulation studies based on the classical molecular dynamics method and combined force and current measurements have shown the relationship between atomic structure and transport properties. The atomic, electronic and transport properties of these nanostructures have been an area of active research. This brief review presents some quantum effects in the electronic and phononic transport through nanowires.

1. Introduction

In our drive towards nanotechnology, there is tremendous interest in understanding the electric and thermal transport through nanowires, as the world moves towards learning the 'physics of small things'. The questions that need to be answered pertain to how the electric and heat transport laws that govern the macroscopic systems get modified at the level of a few molecules or atoms. Wires and contacts having average radius R, in the range of the Fermi wavelength λ_F, can indeed be fabricated and have shown unusual mechanical and electronic properties. The effects of reduced size and dimensionality, and their quantum properties have been investigated actively in the last decade [1]. Ultrathin nanowires [2–8] and even monatomic chains [9, 10] suspended between two metal electrodes have been produced. The discovery of scanning tunnelling microscopy (STM) and later atomic force microscopy (AFM) by Binnig *et al* [11] has sparked a tremendous recent research effort on nanoparticles because

[4] Permanent address: Department of Physics, Bilkent University, Bilkent, Ankara 06533, Turkey.

many properties have become 'directly' observable. The tunnelling microscope has also made it possible to produce atomic size contacts [2–4] and atomic wires only several ångströms in length [7, 10]. Electrical conduction and force have been measured concomitantly in the course of stretching of nanowires [12, 13]. Initially, much of the work was carried out on GaAs–AlGaAs heterostructures which were grown to contain a thin conducting layer at the interface [14, 15]. The conducting layer is treated as a two-dimensional (2D) electron gas in which a narrow constriction of desired width w, and length l, can be created by applying a negative gate voltage.

The conductivity σ, which relates the electric current density to the electric field by $\boldsymbol{j} = \sigma \boldsymbol{E}$, is expressible in terms of the areal charge density ρ_S for 2D electron gas of effective mass m^* through the equation [16]

$$\sigma = \frac{\rho_S e^2 \tau}{m^*}. \tag{1}$$

The experimental quantity of interest, however, is the conductance $G = \mathcal{I}/V$, which is the ratio of the total current $\mathcal{I}$ to the voltage drop V across the sample of length l in the direction of current flow. For 2D, since $\mathcal{I} = wj$, one can also write

$$G = \sigma \frac{w}{l}. \tag{2}$$

For a 3D conductor, this relationship is valid provided that w is replaced by the cross sectional area A orthogonal to the current flow direction. Similar expressions are also valid for the thermal transport of energy. The thermal conductance related to the energy (or heat) current $\mathcal{J}_x$ through a sample between two reservoirs is given by $\mathcal{K}_x = \mathcal{J}_x \Delta T$, where ΔT is the temperature difference [16, 17]. Depending on whether the energy is carried by electrons ($x = e$) or by phonons ($x = p$) the thermal conductance is identified as electronic $\mathcal{K}_e$ or phononic $\mathcal{K}_p$. Here our focus is on quantum transport through materials of very small dimensions.

Novel size-dependent effects emerge as w and l are reduced towards atomic dimensions in the nanometre range. The relationship expressed by equation (2) holds in the diffusive transport regime where both w and l are greater than the mean free path. As the width of the constriction decreases, there comes a point where quantum mechanics makes its presence known. The quantum confinement of a carrier in a strip of width w leads to the discretization of energy levels given by $\epsilon_n = n^2 h^2 / (8m^* w^2)$. The number of these w-dependent transverse modes, which are occupied, determines the conductance. Thus, rather than a simple linear dependence of G on w, quantum mechanics forces this 'indirect' dependence on w. As w is altered, the energy spectrum changes and so does the number of occupied modes below the Fermi energy and hence the conductance.

Simple physical considerations show that the number of transverse occupied states, $N \sim 2w/\lambda_F$, increases with the width of the constriction. Since all these modes can contribute to the conductance, one still expects the conductance to increase linearly with w even in the nanodomain. This is almost the case, except with one important distinction. The width w can change continuously, at least in principle. But the number of modes, being an integer, can only vary in discrete steps. The concept becomes physically more transparent if we rewrite $N \sim n\sqrt{E_F/\epsilon_n}$. The highest occupied $\epsilon_N = E_F$ gives N from a simple counting of the number of discrete eigenvalues. Since it is a rare coincidence for an eigenvalue to exactly align with the Fermi energy, N is taken to be the integer which corresponds to the highest occupied level just below E_F. Thus the effect of quantum mechanics due to the reduced dimension w is to cause the conductance to change in discrete steps in a staircase fashion. We have yet to find the step height. This simple view is necessarily modified when other factors explained in section 2 start to play a crucial role. Obviously, one then requires a more detailed analysis.

The characteristic length that comes into play is λ_F, since only those electrons having energy close to the Fermi energy carry current at low temperatures. If $w \gg \lambda_F$, the number of conducting modes is very large and so is the conductance. This is typical in metals where $\lambda_F \sim 0.2$ nanometres is very small and consequently the observation of discrete conductance variation requires $w \sim \lambda_F$. That is why the discrete conductance behaviour was first observed in semiconductor heterojunctions having very low electron density and λ_F two orders of magnitude larger than in metals [14, 15].

The effect of reduced length l on the conductance is even more striking. If the ohmic regime were to hold in equation (2), one would expect G to increase without limit (or resistance to reach zero) as l was reduced towards zero. We shall see that there would always be finite residual resistance. This was shown by Batra [18] using Heisenberg's uncertainty principle and will be discussed below. A natural characteristic length is the mean free path l_e. If $l < l_e$, carriers can propagate without losing their initial momentum, and this domain is referred to as the ballistic transport regime. Landauer [19] pointed out that 'conduction is transmission'. If we follow the standard definition, that the conductance is a measure of current through a sample divided by the voltage difference,

$$G = \frac{\mathcal{I}}{\Delta V} \tag{3}$$

we can show that the quantum of electrical conductance occurs naturally as a consequence of Heisenberg's uncertainty principle [18]. The current is given by the rate of charge flow $\mathcal{I} = \Delta Q / t_{transit}$. Now charge is quantized in units of elementary charge, e. Hence in the extreme quantum limit, setting $\Delta Q = e$ and recognizing that the transit time should then be at least in the range of time implied by Heisenberg's uncertainty principle, we get

$$\mathcal{I} = \frac{e}{\Delta t}. \tag{4}$$

Combining equation (3) and equation (4), and using the fact that the potential difference, ΔV, is equal to electrochemical potential difference ΔE divided by the electronic charge e, one gets

$$G = \frac{e^2}{\Delta E\,\Delta t}. \tag{5}$$

Next invoking Heisenberg's uncertainty principle, $\Delta E\,\Delta t \geqslant h$, the expression for ballistic conductance including the spin degeneracy becomes $G = 2e^2/h$ in the ideal case. It has a maximum value of $8 \times 10^{-5}\ \Omega^{-1}$. This is the step height, the conductance per transverse mode. The corresponding resistance $h/2e^2$ has a value of 12.9 kΩ (it suffices to call it 12 345 Ω for ease of remembrance) and is attributed to the resistance at the contacts where the conductor is attached to the electrodes or electron reservoirs. Thus classically $G \propto w$. Quantum mechanically it increases in discrete steps. It jumps by $2e^2/h$ as w increases enough to permit one more transverse mode to be occupied and hence available for conduction. A formal description of the step structure will be presented in section 2. More recently, the electronic and transport properties of metallic point contacts and wires having average dimension in the range of metallic λ_F produced by STM [2–5, 7] and also by mechanical break junctions [6] have displayed various quantum effects [20–43]. The two-terminal electrical conductance, G, of the wire showed a stepwise variation with the stretch. The sudden jumps of conductance in the course of the stretch have been taken as the realization of quantized conductance at room temperature and thus have created much popular interest.

Metallic carbon nanotubes providing two conductance channels at the Fermi level are considered almost perfect one-dimensional (1D) conductors. These tubes [44], which can be grown to several micrometres in length with a variety of diameters and chirality, display

unique electromechanical properties and dimensionality effects [45–57]. They can be either semiconductor or metal depending on their chirality and diameter [45–47]. The nanotubes are flexible, and at the same time are very strong with high yield strength. Their strength far exceeds that of any other fibre. These properties are being actively explored with a view to novel applications in nanotechnology. It has been demonstrated experimentally that an individual nanotube can sustain very high current density; first the current increases with the bias voltage and it eventually saturates at a value which is very high for a nanowire [56]. Recent studies have shown that the electronic properties of semiconducting carbon nanotubes can be modified variably and reversibly by radial deformation—a feature that may lead to some device applications [58–60].

The thermal conductance may exhibit quantum features depending on the size of the nanostructure that transfers the phononic energy. Owing to the finite level spacing of vibrational frequencies, the phononic energy transfer through an electrically non-conducting nano-object (i.e. a molecule, atomic chain, or a single atom) between two reservoirs shows behaviour similar to the ballistic electron transport. Recent theoretical studies indicate that the thermal conductance of an acoustic branch at low temperature is independent of any material property, and is linearly dependent on temperature [61–64]. It has also been shown [65] that at low temperature the discrete vibrational frequency spectrum of a 'chain' gives rise to a sudden increase of the thermal conductance.

Study of quantum effects in 1D conductors has seen a tremendous explosion because of growing interest in nanoscience and the quest for novel nanodevices. The scope of this review article is therefore necessarily limited. The subject matter that we have left out is in no way less significant than what we have included. The choice is simply due to our lack of expertise compounded by space limitations. In section 2 we discuss some theoretical methods used in the calculation of quantum transport. The electrical conductance through metallic nanowires is discussed in section 3. After a brief description of the structure and electronic properties, recent experimental and theoretical investigation on the electronic transport through single-wall carbon nanotubes (SWNTs) is reviewed in section 4. The nanotube junctions and other device applications are also introduced in the same section. The electronic and phononic transfer of energy through nanowires and associated quantum effects are discussed in section 5 with some conclusions being given in section 6.

2. Quantum transport of electrons through a constriction

In 1957, Landauer [19] introduced a novel way of looking at conduction. He taught us to view the conduction as transmission and gave the famous formula, which has been a breakthrough in the conductance phenomena and in the physics of mesoscopic systems. According to Landauer, the conduction is a scattering event, and the transport is the consequence of the incident current flux. On the basis of the self-consistency arguments for reflections and transmissions, he derived his famous formula for a one-dimensional conductor yielding the conductance $G = (2e^2/h)\mathcal{T}/\mathcal{R}$, where $\mathcal{T}$ and $\mathcal{R} = 1 - \mathcal{T}$ are transmission and reflection coefficients, respectively. Later, Sharvin [66,67] investigated the electron transport through a small contact between two free-electron metals. Since the length of the contact is negligible, i.e. $l \to 0$, the scattering in the contact was absent and hence $\mathcal{T} \sim 1$. By using a semiclassical approach he found an expression for the conductance, $G_S = (2e^2/h)(Ak_F^2/4\pi)$, which has come to be known as Sharvin's conductance.

The original Landauer formula, i.e. $G = (2e^2/h)\mathcal{T}/\mathcal{R}$, and Sharvin's conductance have seemed to be at variance, since the former yields $G \to \infty$ as $\mathcal{R} \to 0$ in the absence of scattering. The confusion in the literature has been clarified by recognizing the fact that the original formula

is just the conductance of a barrier in a 1D conductor. Engquist and Anderson [68] pointed out an interesting feature by arguing that the conductance has a close relation with the type of measurement. Landauer's formula was extended [69–71] to the conductance measured between the two outside reservoirs within which the finite-length conductor is placed. The corresponding two-terminal conductance formula, $G = (2e^2/h)\mathcal{T}$, incorporates the resistance due to the contacts to the reservoirs. Accordingly, for perfect transmission, $\mathcal{T} \sim 1$, the conductance is still finite and equal to $2e^2/h$. The corresponding resistance $R = G^{-1} = h/2e^2$ is attributed to the resistance arising from the reflections at the contacts where the finite-length conductor is connected to the reservoirs [70, 72]. This leaves unanswered the question of how the contact resistance can be independent of the type of contact. Also the infinite conductance within the conductor at perfect transmission requires an in-depth discussion. Whether the finite conductance of an ideal channel, $2e^2/h$, is due to the contact or due to the capacity of the current-transporting state seems to be a matter of interpretation.

Büttiker [73] developed the multi-probe generalization of the theory. During the last decade, important progress has been made in mesoscopic physics; the quantum transport of electrons through constrictions has been a subject of many in-depth studies [72]. In particular, the variation of the current through a point contact created by an STM tip [2] and the measurements of the conductance G through a narrow constriction between two reservoirs of 2D electron gas in a high-mobility GaAs–GaAlAs heterostructure [14, 15] showing step behaviour with a step height of $2e^2/h$ have led to basic confirmation of Landauer's fundamental ideas.

The step behaviour of G has been treated in several studies [74–78]. Further to our arguments in section 1, here we provide a simple and formal explanation by using a 1D idealized uniform constriction having a width w. The electrons are confined in the transverse direction and have states with quantized energy ϵ_i. They propagate freely along the length of the constriction. The propagation constant for an electron with $\epsilon_i < E_F$ is

$$\gamma_i = \left[\frac{2m^*}{\hbar^2}(E_F - \epsilon_i) \right]^{1/2}.$$

Whenever the width of the constriction increases by $\lambda_F/2$, a new subband with energy $\epsilon_i + \hbar^2\gamma_i^2/2m$ dips below the Fermi level and contributes to the current under the small bias voltage ΔV. The current is

$$I = \sum_{i=1}^{j} 2n_i e v_{\gamma_i}[\mathcal{D}_i(E_F + e\,\Delta V) - \mathcal{D}_i(E_F)]. \tag{6}$$

Here j is the index of the highest subband that lies below the Fermi level, i.e. $\epsilon_j \leqslant E_F + e\Delta V$ and $\epsilon_{j+1} > E_F + e\Delta V$, and n_i is the degeneracy of the state i. By assuming perfect transmission in the absence of any contact resistance and barrier inside the constriction, i.e. $\mathcal{T} = 1$, and by expressing the group velocity v_{γ_i} and the density of states $\mathcal{D}_i(\epsilon)$ in terms of the subband energy $\epsilon = \epsilon_i + \hbar^2\gamma_i^2/2m^*$ and dividing I by ΔV we obtain

$$G = \sum_{i=1}^{j} \frac{2e^2}{h}n_i. \tag{7}$$

Accordingly, each current-transporting state with energy in the range $E_F < \epsilon < E_F + e\,\Delta V$ contributes to G an amount $2e^2 n_i/h$.

For a uniform, infinite wall constriction, the states are non-degenerate, i.e. $n_i = 1$, and hence the increase of w by $\lambda_F/2$ causes G to jump by $2e^2/h$. As a result, the $G(w)$ curve exhibits a staircase structure. Since the level spacing in the transverse quantization is rather

small for the low electron density in the 2D electron gas system, and $\Delta\epsilon \sim \lambda_F^{-2}$, the sharp step structure is likely to be smeared out at $T \sim 10$ K or at finite bias voltage [24, 79, 80].

For a finite-length constriction the scattering at the contacts to the reservoirs (i.e. the contact resistance) [81, 82] and at the non-uniformities [83, 84] or the potential barriers inside the constriction [85] affect the transmission. Then, the conductance of a single channel expressed as

$$G = (2e^2/h)\mathcal{T} \tag{8}$$

may deviate from the perfect quantized values. As a result, the effects, such as the contact and potential barrier [24, 81, 82, 85], surface roughness [84], impurity scattering [83, 86–89], cause the sharp step structure of $G(w)$ to smear out. The local widening of the constriction or impurity potential can give rise to quasi-bound (0D) states in the constriction and to resonant tunnelling effects [84, 90, 91].

The length of the constriction, l, is another important parameter. In order to get sharp step structure, l has to be greater than λ_F, but smaller than the electron mean free path l_e; $G(w)$ is smoothed out in a short constriction ($l < \lambda_F$). Therefore, $G(w)$ exhibits sharp step structure if the constriction is uniform, and $w \sim \lambda_F$ and $\lambda_F \ll l < l_e$. On the other hand, the theoretical studies predict that the resonance structures occur on the flat plateaus due to the interference of waves reflected from the abrupt connections to the reservoirs [24, 77]. The stepwise variation of G with w or E_F has been identified as the quantization of conductance. This is, in fact, the reflection of the quantized constriction states in the electrical conductance.

We now extend the above discussion to analyse the ballistic electron conductance through a point contact or a nanowire, in which the electronic motion is confined in two dimensions, but freely propagates in the third dimension. The point contact (or quantum contact) created by the indentation of the STM, a nanowire (or a connective neck) that is produced by retracting the tip from an indentation [2] and also a metallic SWNT are typical systems of interest. Nanowires created by STM are expected to be round (though not perfectly cylindrical) and have radius $R \sim \lambda_F$ at the neck. The neck is connected to the electrodes by horn-like ends, and hence the radius increases as one goes away from the neck. An extreme case for $l \to 0$ is Sharvin's conductance [26, 66], $G_S = (2e^2/h)(\pi R/\lambda_F)^2$, with contact radius R, where the step structure is almost smeared out and plateaus disappear. In the quantum regime, where the cross section $A \sim \lambda_F^2$, G_S should vanish when A is smaller than a critical cross section set by the uncertainty principle. As l increases, a stepwise behaviour for G_S develops [24].

The real point contacts and metallic nanowires differ from the perfect uniform constriction in the way that the electrons are quantized in the neck. The size and form of the neck, and also its electronic potential, influence the quantization of the electronic states and the level spacing. The form of the neck may be irregular if the cross section is large and comprises few atoms, but shows cylindrical symmetry for an undeformed SWNT or metallic nanowire having a single atom at the neck. The cylindrical symmetry becomes apparent with the degeneracy [22, 26, 92] $n_i = 1, 2, 2, 1, \ldots$ for $i = 1, 2, 3, 4, \ldots$. For the most general constriction the expression for the two-terminal conductance in equation (3) is generalized to the form [70, 93]

$$G = \frac{2e^2}{h}\text{Tr}(\mathbf{t}^+\mathbf{t}) \tag{9}$$

where the elements of the transmission matrix $\mathbf{t}$, t_{ij}, are the amplitudes of transmission from the incoming channels to the outgoing ones. In actual electron transport through a contact or wire, the electrons of the electrodes with proper representation (say in Bloch form) enter in the constriction, and pass to the other electrode after multiply scattering from the walls or from other scattering centres in the constriction [94]. In the steady state the potential of the wire can be different from that in the case of a self-consistently calculated potential under

zero-current conditions. Therefore, full calculation of the conductance based on the density functional theory has to start with the actual states of the electrodes and evaluate the **t**-matrix for the self-consistent potential under the steady-state current flow. Various methods at different levels of sophistication have been applied to calculate the conductance.

The simplest model for representing a nanowire or point contact is a cylindrical or circular hard-wall potential with varying radius, $R(z)$. The axis of the constriction is along the z-direction; the x- and y-axes are in the transverse plane [24]. An approach alternative to the circular cross section is the rectangular cross section [5] with sides $L_x(z)$ and $L_y(z)$, both varying smoothly with z. Many studies employed these models to show the step behaviour of the conductance. The potential of the constriction corresponding to a given atomic structure which was omitted in these model studies has been taken into account first by performing SCF electronic structure calculations [22, 24, 82], or by obtaining the potential from the linear combination of atomic potentials [35, 36]. Then, the calculated potential is approximated by a potential having cylindrical symmetry:

$$V_l(\rho, z) = \phi_l(z) + \alpha_l(z)\rho^2 \tag{10}$$

throughout the constriction. Here l is the length of the constriction, and $\rho = (x^2 + y^2)^{1/2}$. The saddle point potential $\phi_l(z)$ is an essential ingredient which was omitted in the calculations using the hard-wall potential. The current-transporting state $\Psi_{k_i}(\rho, z)$ corresponding to the incident plane wave $\mathrm{e}^{\mathrm{i}k_i \cdot r}$ of energy $E = \hbar^2 k_i^2/2m^*$ is written as a linear combination of the longitudinal and transverse states:

$$\Psi_{k_i}(\rho, z) = \sum_n [A_{n_{k_i}}(z)\mathrm{e}^{\mathrm{i}\gamma_n(z)z} + B_{n_{k_i}}(z)\mathrm{e}^{-\mathrm{i}\gamma_n(z)z}]\Phi_n(\rho, z) \tag{11}$$

where the transverse state $\Phi_n(\rho, z)$ is the 2D harmonic oscillator solution for a given $\alpha_l(z)$ with $n = n_x + n_y$ and energy $\epsilon_{n,l}(z) = (n + 1)[2\hbar^2\alpha_l(z)/m^*]^{1/2}$. The propagation constant is given by

$$\gamma_n(z) = \frac{2m}{\hbar^2}[E - \phi_l(z) - \epsilon_{n,l}(z)].$$

The conductance of the wire is calculated by using the transfer-matrix method, where $V_l(\rho, z)$ is divided into discrete segments of equal widths, and in each segment $z_j < z < z_{j+1}$, the average values are used. The coefficients $A_{n_{k_i}}$ and $B_{n_{k_i}}$ are determined from the multiple boundary matching conditions. The total conductance is calculated by integrating the expectation value of the current operator over the Fermi surface [82].

A constriction having more general geometry and potential can be treated by expressing the current-transporting state in the Laue expansion

$$\Psi_j(\rho, z) = \sum_n \mathrm{e}^{\mathrm{i}G_n \cdot \rho} f_{n,j}(z)$$

in terms of transverse reciprocal-lattice vectors, G_i. This method is convenient when using the SCF potentials obtained from supercell calculations. Furthermore, the conductance of rather long constrictions calculated by using the recursion scheme do not diverge. The Schrödinger equation for Ψ_j is discretized in the segments $z_j < z < z_{j+1}$, and converted to a matrix equation. The details of the calculations can be found elsewhere [33, 95].

The Green's function method has been used extensively to study the electrical conduction through nanowires [25, 27, 28, 32] and also SWNTs [72, 96]. In the self-consistent calculation [28], where the wave functions of the bare electrodes, Ψ^0, are evaluated from a realistic Hamiltonian, the wave functions of the complete system including the constriction, Ψ^C, are put into the Lippmann–Schwinger form:

$$\Psi^C(r) = \Psi^0(r) + \int \mathrm{d}r' \, \mathrm{d}r'' \, G^0(r, r')\delta V(r', r'')\Psi^C(r) \tag{12}$$

where δV is the potential difference between the complete and bare systems, and G^0 is the Green's function obtained for the bare system. In the work by Lang [28] the electrodes are treated in the jellium approximation, and the potentials at the constriction due to metal atoms are expressed by the pseudopotentials. Once Ψ^0 and Ψ^C are expressed in the plane-wave representation, the currents between the electrodes in the presence and in the absence of the constriction are obtained from the expectation value of the current operator by summing over all the states of the jellium electrodes under the bias $e\,\delta V$. The calculations using the Laue-type expansion [95] have indicated that the division of the current-transporting state in the electrode by jellium and in the wire by pseudopotential, which essentially neglects the binding structure at the entrance to the reservoirs, may not fully describe the real physical system.

In the Green's function method within the tight-binding representation using empirical energy parameters, a conducting nanowire or a nanotube is divided into three parts [72, 96]. These are the left (L), right (R) and central (C) regions; the left and right regions are coupled to two semi-infinite leads. The central region is the computationally important part which may include tube junctions, defects or vacancies. Partitioning the Green's function into submatrices due to the left, right and central regions, one can obtain the Green's function for the central region as

$$\mathcal{G}_C^r = (\epsilon - H_C - \Sigma_L - \Sigma_R)^{-1}. \tag{13}$$

The self-energy terms, Σ_L and Σ_R, describe the effect of semi-infinite leads on the central region. The functions for the coupling can be obtained as $\Gamma_{L,R} = i[\Sigma_{L,R}^r - \Sigma_{L,R}^a]$ in terms of the retarded (r) and advanced (a) self-energies. An important part of the problem is calculating the self-energy terms. The surface Green's function matching method [96–98] or computational algorithms [99] are used to calculate the Green's functions of semi-infinite leads and the self-energy terms. These terms can be obtained by using wave functions of ideal leads also [72]. The transmission function $\mathcal{T}$, that represents the probability of transmitting an electron from one end of the conductor to the other end, can be calculated using Green's functions of the central region and couplings to the leads:

$$\mathcal{T} = \mathrm{Tr}(\Gamma_L \mathcal{G}_C^r \Gamma_R \mathcal{G}_C^a). \tag{14}$$

Here $\mathcal{G}_C^{r,a}$ are the retarded and advanced Green's functions of the centre, and $\Gamma_{L,R}$ are functions for couplings to the leads. This approach is used efficiently to treat nanotube junctions and nanodevices as discussed in section 4. Note that the success of the approach depends on the transferability of the empirical energy parameters.

3. Electrical conduction through nanowires

An atomic size contact and connective neck first created by Gimzewski and Möller [2] by using a STM tip exhibited abrupt changes in the variation of the conductance with the displacement of the tip. Initially, the observed behaviour of the conductance was attributed to the quantization of conductance. At that time, from calculating the quantized conductance of a perfect but short connective neck, Ciraci and Tekman [22] concluded that the observed abrupt changes of the conductance can be related to the discontinuous variation of the contact area. Later, Todorov and Sutton [25] performed an atomic scale simulation of indentation based on the classical molecular dynamics (MD) method and calculated the conductance for the resulting atomic structure using the s-orbital tight-binding Green's function method. They showed that sudden changes of conductance during indentation or stretching are related to the discontinuous variation of the contact area. Recently, nanowires of better quality have been produced using STM by Agräit *et al* [3], Pascual *et al* [4, 7] and Olesen *et al* [5], and also by using the

mechanical break junction by Krans *et al* [6]. The two-terminal electrical conductance of these wires showed abrupt changes with the stretching.

The radius of the narrowest cross section of the wire prior to the break is only a few ångströms; it has the length scale of λ_F, where the discontinuous (discrete) nature of the metal dominates over its continuum description. Since the level spacing $\Delta\epsilon$ is in the region of ~ 1 eV at this length scale, the peaks of the density of states $D(\epsilon)$ of the connective neck become well separated and hence the transverse quantization of states becomes easily resolved even at room temperature. Furthermore, any change in the atomic structure or the radius induces significant changes in the level spacing and in the occupancy of states. This, in turn, leads to detectable changes in the related properties. Therefore, the ballistic electron transport through a nanowire should be closely related to its atomic structure and radius at its narrowest part. On the other hand, irregularities of the atomic structure and electronic potential enhance scattering that destroys the regular staircase structure [83]. In the following section, we summarize results that emerged from recent experimental and theoretical studies on stretched nanowires.

3.1. Atomic structure and mechanical properties

Computer simulations of the atomic structure of connective necks created by STM were first performed in the seminal works by Sutton and Pethica [100], and Landman *et al* [101]. It was noted that the deformation (or elongation) generally occurred in two different and consecutive stages that repeat while the wire is stretched [33, 36, 101]. In the first stage, which was identified as *quasi-elastic*, the stored strain energy and average tensile force increase with increasing stretch s, while the atomic layers are maintained. The variation of the applied tensile force, $F_z(s)$, in this stage is approximately linear, but it deviates from linearity as the number of atoms in the neck decreases. Fluctuations in $F_z(s)$ can occur possibly due to displacement and relocation of atoms within the same layer or *atom exchange* between adjacent layers. Also, intralayer and interlayer atom relocations can give rise to conductance fluctuations [36].

The second stage that follows each quasi-elastic stage is called the *yielding* stage. A wire can yield by different mechanisms depending on its diameter. The motion of the dislocation and/or the slips on the glide planes are generally responsible for the yielding if the wire maintains an ordered (crystalline) structure and has a relatively large cross section. The type of the ordered structure and its orientation relative to the z-axis (or stretching direction) are expected to affect the yielding. On the other hand, as predicted by MD simulations, yielding can occur by *order–disorder transformation* [27, 36, 101] and *single-atom exchange* [35, 36] if the cross section of the wires is relatively small. Once the elongation reaches approximately the interlayer spacing at the end of the quasi-elastic stage, the structure becomes disordered. But after further stretching, it recovers with the formation of a new layer. In the yielding stage, $|F_z|$ decreases abruptly; the cross section of the layer formed at the end of the yielding stage is abruptly reduced by a few atoms. As a typical example, the force variation and atomic structure calculated by the MD method are illustrated in figure 1. When the neck becomes very narrow (having 3–4 atoms), the yielding is realized, however, by a single atom jumping from one of the adjacent layers to the interlayer region.

Under certain circumstances, atoms at the neck form a *pentagon* that becomes staggered in different layers [36]. The interlayer atoms make a chain passing through the centre of the pentagon rings. In this new phase, the elastic and yielding stages are intermixed and elongation, which is by more than one interlayer distance, can be accommodated. As the cross section of the wire is further decreased the pentagons are transformed to a *triangle*. In the initial stage of pulling off, the single-atom process, in which individual atoms also migrate from central layers towards the end layers, can give rise to a small and less discontinuous change in the
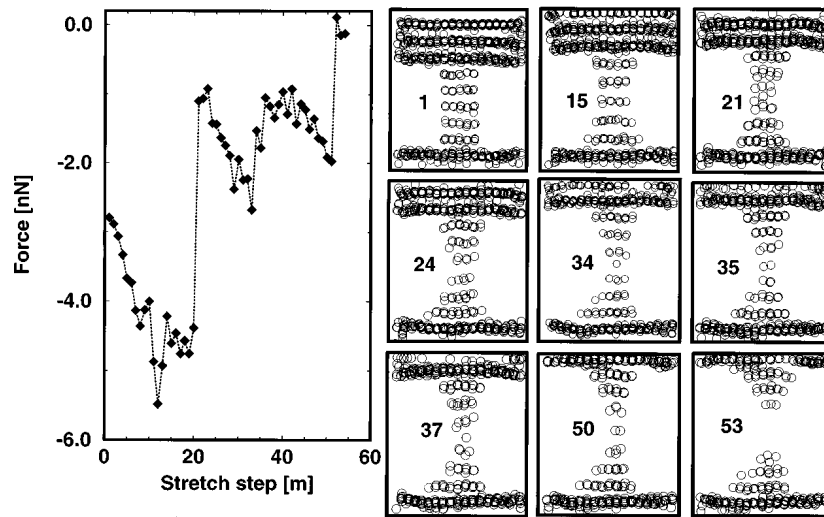
Figure 1. The variation of the tensile force F_z (in nanonewtons) with the strain or elongation s along the z-axis of the nanowire having Cu(001) structure. The stretch s is realized in m discrete steps. The snapshots show the atomic positions at relevant stretch steps m. The MD simulations are performed at $T = 300$ K. (Reproduced from reference [36].)

cross section. The tendency to minimize the surface area, and hence to reduce the strain energy of the system, is the main driving force for this type of neck formation. While quasi-elastic and yielding stages are distinguishable initially, the force variation becomes more complex and more dependent on the migration of atoms for atomic necks. Atomic migrations have important implications such as dips in the variation of conductance with stretch. The simulation studies on metal wires with diameters $\sim\lambda_F$ at the neck, but increasing gradually as one goes away from the neck region, have shown structural instabilities. Such wires displayed spontaneous thinning of the necks even in the absence of any tensile strain [35, 36]. This result, though puzzling, is in agreement with the experiment done by using the mechanical break junction method on a gold neck at room temperature that broke by itself [31].

Under prolonged stretching, shortly before the break, the cross section of the neck is reduced to include only 2–3 atoms. In this case, the hollow-site registry may change to the top-site registry. This leads to the formation of a *bundle of atomic chains (rope)* or of a *single atomic chain* (see figure 2). We consider this a dramatic change in the atomic structure of the wire that has important implications. For example, first-principles calculations indicated that a chain of single Al atoms has an effective Young modulus stronger than that of the bulk [36]. The predictions by Mehrez and Ciraci [35, 36] regarding the formation of a rope and an atomic chain at the neck have been confirmed experimentally. Using an ultrahigh-vacuum electron microscope, Ohnishi *et al* [9] observed 'strands' and a single chain of gold atoms suspended between two gold electrodes. They deduced interatomic distances (as large as 3.5 to 5 Å) much larger than the bulk value. Recently, the structure and the stability of gold chains between two electrodes have been the subject of extensive calculations. The first-principles density functional calculations by Portal *et al* [102] found that a zigzag structure of seven gold atoms between two gold electrodes is energetically favourable and can explain the field-emission images [9]. On the other hand, calculations by Häkkienen *et al* [103] favour the dimerization of the linear chain. It appears that the atomic arrangements of the electrodes where the chain is connected are crucial in determining the atomic structure of the monatomic chain. The
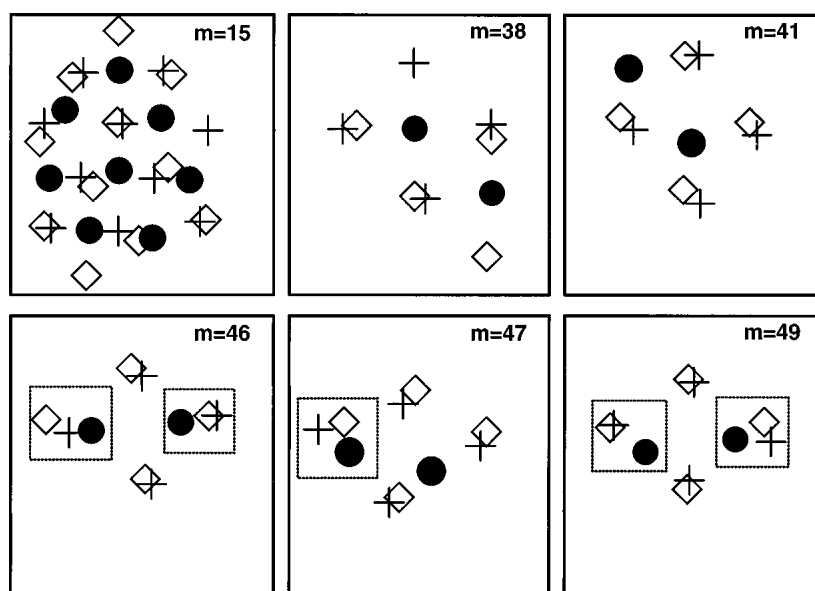
Figure 2. The top view of three layers at the neck showing atomic positions and their relative registry at different levels of stretch. $m = 15$ occurs before the first yielding stage. The atomic positions in the layers 2, 3 and 4 are indicated by $+$, $\bullet$ and $\diamond$, respectively. $m = 38$ and $m = 41$ occur after the second yielding stage. $m = 46, 47$ and $m = 49$ show the formation of bundle structure (or strands). In the panels for $m = 38$–49 the positions of atoms in the third, fourth and fifth (central) layers are indicated by $+$, $\bullet$ and $\diamond$, respectively. Atomic chains in a bundle are highlighted by square boxes. (Reproduced from reference [36].)

zigzag structure forming equilateral triangles is favoured for a 1D infinite metallic chain since the number of nearest neighbours increases from two (corresponding to an undimerized linear chain) to four. Nevertheless, several questions remain to be clarified in future studies:

 (i) Why does a metal chain form a zigzag structure?
 (ii) Are there other lower energy structures indigenous to one-dimensional systems?
(iii) Why is the gold chain stable while other metal monatomic chains appear to be unstable under strain?
(iv) How does the conductance depend on the structure of the chain?
 (v) How does the current flow affect the stability of the chain?

Recent computer simulations [104] have suggested that ultrathin lead wires should develop exotic, non-crystalline stable atomic structures once their diameter decreases below a critical size of the order of a few atomic spacings. The new structures, whose details depend upon the material and the wire thickness, may be dominated by icosahedral packings. Helical, spiral-structured wires with multi-atom pitches are also predicted. Recently, helical multi-shell gold nanowires were observed by high-resolution electron microscopy by Kondo and Takayanagi [105]. The phenomenon, analogous to the appearance of icosahedral and other non-crystalline shapes in small clusters, can be rationalized in terms of surface energy anisotropy and optimal packing. Moreover, the electronic structure of the wire might carry a measurable imprint of its exotic shape. Studies of exotic atomic structure of ultrathin nanowires and associated physical properties are important for future advances [106].

3.2. Electrical conductance of nanowires

The overall features of electrical conductance have been obtained from a statistical analysis of the results of many consecutive measurements to deduce how frequently a measured conductance value occurs. Many distribution curves exhibited a peak near $G_0 = 2e^2/h$ for metal nanowires, and a relatively broad peak near $3G_0$, and almost no significant structure for larger values of conductance. It appears that the cross section of a connective neck can be reduced down to a single atom just before the wire breaks. In certain situations, the connective neck can be a monatomic chain comprising of a few atoms arranged in a row. In this case, a transverse state quantized in the neck at the Fermi level is coupled to the states of the electrodes and forms a conducting channel yielding a plateau in the $G(s)$ curve, and hence a peak in the statistical distribution curve. The step structure for large necks comprising of a few atoms cannot occur at integer multiples of G_0 due to the scattering from irregularities, and hence due to the channel mixing [24, 83, 84].

It should be noted that in the course of stretching, elastic and yielding stages repeat; the surface of the nanowire roughens and deviates strongly from circular symmetry. The length of the narrowest part of the neck is usually only one or two interlayer separations, and is connected to the horn-like ends. Under these circumstances, the quantization is not complete and the contribution of the tunnelling is not negligible. Results of atomic simulations [27, 33, 35, 100, 101] point to the fact that neither adiabatic evolution of discrete electronic states, nor perfect circular symmetry can occur in the neck. Consequently the expected quantized sharp structure shall be smeared out by channel mixing and tunnelling. Contradicting these arguments, the changes in the conductance are, however, abrupt. This controversial situation has been explained by the combined measurements of the conductance and force variation with the stretch. It has been shown [12, 13] that the abrupt changes of conductance in the course of stretching coincide with the sudden release (or relief) of the measured tensile force. It is clear from the previous discussion that the tensile stress is released suddenly following the yielding stage, whereby the cross section of the wire is reduced discontinuously, and hence the electronic structure and the electronic level spacing undergo an abrupt change near the neck [22]. The variation of the conductance, i.e. $G(s)$, calculated [35] for stretching the nanowire is presented as an example in figure 3.

Calculations of $G(s)$ corresponding to the atomic structure generated from classical MD simulations were carried out by Todorov and co-workers [27, 32] using the Green's function method within the s-orbital tight-binding approximation. Barnett and Landman [107] performed similar calculations on the Na nanowires by using MD based on the *ab initio* electronic structure calculations. They found that the conductances of these nanowires exhibit dynamical thermal fluctuations on a subpicosecond timescale owing to rearrangements of the metal atoms explained in section 3.1. The giant conductance fluctuation, i.e. $G_{max}/G_{min} \sim$ 10–15, is rather surprising, and perhaps is due to the artifact of applying Kubo–Greenwood formalism for a finite system [108, 109].

The density of states of a perfect 1D atomic wire can be expressed as

$$D(\epsilon) = \sum_i \theta(\epsilon - \epsilon_i)(\epsilon - \epsilon_i)^{-1/2}.$$

It has peaks at the quantized energies of transversely confined states, i.e. when $\epsilon = \epsilon_i$. The occupancy of these states becomes strongly dependent on the size and the geometry of the wire. Sudden reduction in the ballistic conductance will occur whenever a channel is closed (i.e. a current-transporting state moves above the Fermi energy, E_F). Also, whenever the tensile force along the axis of the wire $|F_z|$ shows a sudden fall, it is possible that the actual R (or the narrowest cross section, A) experiences a change only at certain positions of ϵ_i relative
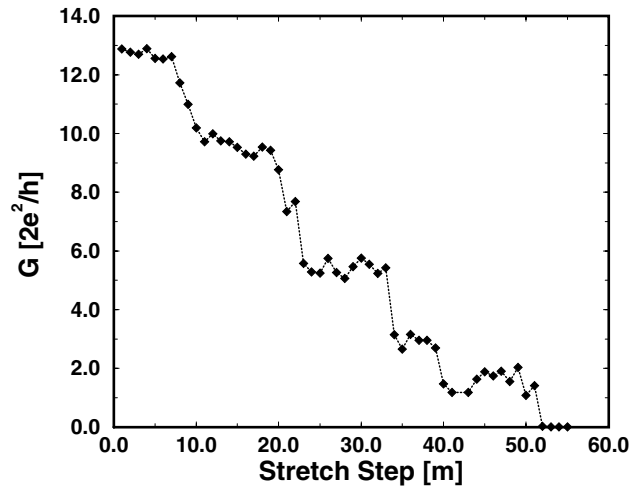
Figure 3. Variation of the conductance calculated for the stretching nanowire described in figure 1. (Reproduced from reference [36].)

to E_F. Such a possibility was pointed out on the basis of earlier works indicating quantum size effects [36]. In fact, it is known that the surface energy, work function etc for a 2D electron system show discrete changes as the relevant size (or thickness) changes [110, 111]. This is explained by noting that the increase occurs when an empty band gets occupied as a result of size change. Similar effects have been reported for clusters treated in the jellium approximation [112]. Stafford *et al* [113] showed that in fact abrupt changes in conductance and diameter of a uniform wire are correlated, so certain values of R or A are energetically favourable as if the size is 'quantized'.

3.3. Electrical conductance through a single atom

The conductance through a single atom, a nanowire with the ultimate small cross section, has provided fundamental understanding. On the basis of *ab initio* calculations it has been shown that the conductance depends on the valence states as well as the site where the single atom is bound to the electrode [37]. The coupling to electrodes and hence the transmission coefficients are expected to depend on the binding structure. Scheer *et al* [114] found a direct link between valence orbitals and the number of conduction channels in the conductance through a single atom. Lang [34] calculated the conductance through a single Na atom, as well as a monatomic chain comprising two, three and four Na atoms between two jellium electrodes by using the Green's function formalism. He found an anomalous dependence of the conductance on the 'length' of the wire. The conductance through a single atom was low ($\sim G_0/3$), but increased by a factor of two in going from a single atom to the two-atom wire. This behaviour was explained as the incomplete valence resonance of a single Na atom interacting with the continuum of states of the jellium electrodes. Each additional Na atom modifies the electronic structure and shifts the energy levels. The closer a state is to the Fermi level, the higher is its contribution to the electrical conductance. According to the Kalmeyer–Laughlin theory [115], a resonance with the maximum DOS at the Fermi level makes the highest contribution to the transmission; the conductance decreases as the maximum shifts away from the Fermi level.

This explanation is valid for a single atom between two macroscopic electrodes forming a neck with length $l < \lambda_F$. The situation is, however, different for long monatomic chains. Since

the electronic energy structure of a short monatomic chain varies with the number of atoms, the results are expected to change if one goes beyond the jellium approximation and considers the details of the coupling of chain atoms to the electrode atoms. It is also expected that the conductance will depend on where the monatomic chain (represented by the pseudopotentials) ends and where the jellium edge begins. In fact, Yanson *et al* [10] argued that the conductance of the Na wire calculated by Lang [28] is lower than the experimental value possibly due to the interface with the jellium.

4. Carbon nanotubes

Nanotubes were discovered by Iijima [44] in the form of multiple coaxial carbon fullerene shells (multi-wall nanotubes, MWNTs). Later, in 1993 single fullerene shells (single-wall nanotubes, SWNTs) were synthesized [44, 116] using transition metal catalysts. A nanotube can be simply described as a sheet of graphite (or graphene) coaxially rolled to create a cylindrical surface (as shown in figure 4(a)). In this way the 2D hexagonal lattice of graphene is mapped onto a cylinder of radius R. The mapping can be realized with different helicities resulting in different nanotubes. Each nanotube is characterized by a set of two integers (n, m) indicating the components of the chiral vector $C = n\boldsymbol{a}_1 + m\boldsymbol{a}_2$ in terms of the 2D hexagonal Bravais lattice vectors of graphene, $\boldsymbol{a}_1$ and $\boldsymbol{a}_2$, as illustrated in figure 4(b). The chiral vector is a circumferential vector and the tube is obtained by folding the graphene such that the two ends of C are coincident. The radius of the tube is given in terms of (n, m) through the relation $R = a_0\sqrt{n^2 + m^2 + nm}/2\pi$, where $|\boldsymbol{a}_1| = |\boldsymbol{a}_2| = a_0$. When C involves only $\boldsymbol{a}_1$ (corresponding to $(n, 0)$) the tube is called 'zigzag', and if C involves both $\boldsymbol{a}_1$ and $\boldsymbol{a}_2$ with $n = m$ (corresponding to (n, n)) the tube is called 'armchair' [45]. The chiral (n, n) vector is rotated by $30°$ relative to that of the zigzag $(n, 0)$ tube. SWNTs are found in the form of nanoropes, each rope consisting of up to a few hundred nanotubes arranged in a hexagonal lattice structure [117].
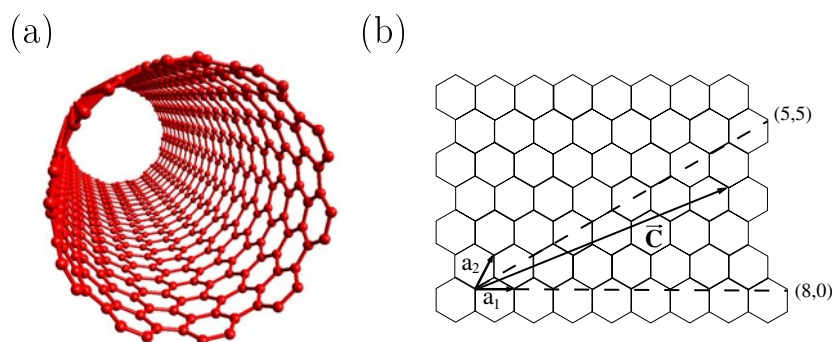

Figure 4. (a) A single-wall nanotube is graphene wrapped on a cylinder surface. (b) Nanotubes are described by a set of two integers (n, m) which indicate the graphite lattice vector components. A chiral vector can be defined as $C = n\boldsymbol{a}_1 + m\boldsymbol{a}_2$. Tubes are called 'zigzag' if either one of the integers is zero $(n, 0)$ or called 'armchair' if both integers are equal (n, n).

4.1. Electronic structure

As a nanotube is in the form of a wrapped sheet of graphite, its electronic structure is analogous to the electronic structure of a graphene [118–120]. Graphene has the lowest π^*-conduction

band and the highest π-valence band, which are separated by a gap in the entire hexagonal Brillouin zone (BZ) except at its K corners where they cross. In this respect, graphene lies between a semiconductor and a metal with *Fermi points* at the corners of the BZ. One can imagine an unrolled, open form of nanotube, which is graphene subject to periodic boundary conditions on the chiral vector. This in turn imposes quantization on the wave vector. This is known as zone folding, whereby the BZ is sliced with parallel lines of wave vectors, leading to subband structure. A nanotube's electronic structure can thus be viewed as a zone-folded version of the electronic band structure of the graphene. When these parallel lines of nanotube wave vectors pass through the corners, the nanotube is metallic. Otherwise, the nanotube is a semiconductor with a gap of about 1 eV, which is reduced as the diameter of the tube increases. Within this simple approach, (n, m) nanotubes are metallic if $n - m = 3 \times$ integer. Consequently, all armchair tubes are metallic. The conclusion that one draws from the above discussion is that the electronic structures of nanotubes are determined by their chirality and diameter, i.e. simply by their chiral vectors C.

The first theoretical calculations were performed and the above simple understanding was provided much earlier than the first conclusive experiments were carried out [118–120]. In these early calculations, a simple one-band π-orbital tight-binding model was used. *Ab initio* methods have also been used to investigate the electronic structure of SWNTs. However, different calculations have been at variance on the values of the band gap. For example, while the σ^*–π^* hybridization due to the curvature can be treated well by *ab initio* calculations [121], simple tight-binding methods may have limitations for small-radius nanotubes. In figures 5(a) and 5(b) the band structure and density of states (DOS) of a (10, 10) tube are given, based on a tight-binding calculation. Samples prepared by laser vaporization consist predominantly of (10, 10) metallic armchair SWNTs. As can be seen in figure 5(a), band crossing is allowed, and the bonding π- and antibonding π^*-states cross the Fermi level at $k_z = 2\pi/3$ [118–120].
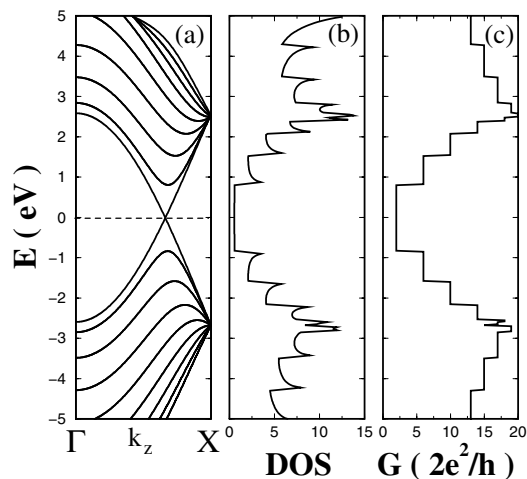

Figure 5. (a) The band structure, (b) density of states and (c) conductance of a (10, 10) nanotube. The tight-binding model is used to derive the electronic structure. The conductance is calculated using the Green's function approach with the Landauer formalism.

In figure 5(b) the density of states is plotted for the (10, 10) tube. The $E^{-1/2}$-singularities which are typical for 1D energy bands appear at the band edges [118]. STM spectra of nanotubes show densities of states with similar singularities to those obtained by band calculations [50, 51]. One-dimensional metallic wires are generally unstable and have Peierls distortion.

The energy gain after Peierls distortion is found to be very small for nanotubes and the Peierls energy gap can be neglected. The curvature of nanotubes introduces hybridization also between sp^2 and sp^3 orbitals, but these effects are small when the radius of a SWNT is large [122]. However, the π^*- and σ^*-state mixing was enhanced for small-radius zigzag SWNTs [121]. Recently, it has been shown that the electronic properties of a SWNT can undergo dramatic changes owing to the elastic deformations [58, 59, 123, 124]. For example, the band gap of a semiconducting SWNT can be reduced or even closed by the elastic radial deformation. The gap modification and the eventual strain-induced metallization seem to offer new alternatives for reversible and tunable quantum structures and nanodevices [60].

4.2. Quantum transport properties

A nanotube can be an ideal quantum wire for electronic transport; two subbands crossing at the Fermi level should nominally give rise to two conducting channels. Under ideal conditions each channel can carry current with unit quantum conductance $2e^2/h$; the total resistance of an individual SWNT would be $h/4e^2$ or ~ 6 kΩ. The contribution of each subband to the total conductance is clearly seen in figure 5(c) illustrating the calculated conductance of the (10, 10) nanotube.

The first electronic transport measurements of nanotubes were carried out using MWNTs [125–127]. These measurements found MWNTs to be highly resistive due to defect scattering and weak localization. The first electronic transport measurements of individual SWNTs and nanoropes were performed by Tans *et al* [53] and Bockrath *et al* [54]. In these measurements nanotubes or nanoropes were placed on an insulating (oxidized silicon) substrate containing metallic electrodes. In figure 6(a) an AFM image of an individual SWNT on a silicon dioxide substrate is shown with two Pt electrodes. A gate voltage V_g is applied to the third electrode in the upper left corner to shift the electrostatic potential of the nanotube. The measurements were performed at 5 mK and step-like features are observed in current–voltage curves shown in figure 6(b). Note that the voltage scale is mV and these steps are not due to the quantized increase of conductance with subbands shown in figure 5(c). These steps are due to resonant tunnelling of electrons to the states of a finite nanotube [53, 54]. The presence of metallic electrodes introduces significant contact resistances and changes the bent part of the nanotube into a quantum-dot-like structure. The same phenomena were seen in individual ropes of nanotubes with oscillations in the conductance at low temperatures [54].

Figure 7 shows conductance versus gate voltage for a nanorope for various temperatures. The average conductance drops with T. Conductance oscillations at low temperatures are due to the Coulomb blockade effect. The energy levels of the rope are quantized and the single molecular level spacing $\Delta\epsilon$ exceeds the thermal energy, $k_B T$ [53, 54]. On changing the gate voltage, single electrons tunnel to the quantized molecular levels. Recently, metallic contacts with low resistances have been achieved [129, 130] which do not show Coulomb blockade oscillations down to 1.7 K. Another important behaviour in figure 7 is the monotonic decrease of conductance with decrease of temperature which is a signature of correlated electron liquids. It is well known that the electrons in one-dimensional systems may form not Fermi liquids but the so-called Luttinger liquids with electron correlation effects [131]. An important feature of Luttinger liquids is the separation of spin and charge by formation of quasi-particles. Theoretical investigations of correlation effects in nanotubes were performed by Kane *et al* [132] and Egger and Gogolin [133]. They argued that electrons in armchair SWNTs form a Luttinger liquid. Bockrath *et al* [134] confirmed these arguments by observing power-law dependences of the conductance on voltage ($G \propto V^\alpha$) and also on temperature ($G \propto T^\alpha$), which are typical for Luttinger liquids.
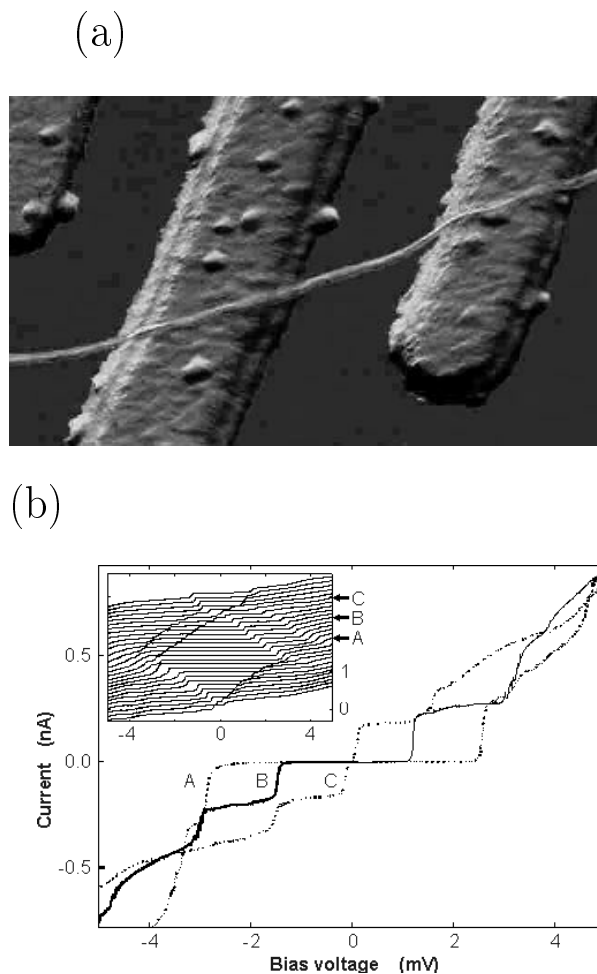
Figure 6. (a) An AFM image of a carbon nanotube on top of a Si/SiO$_2$ substrate with Pt electrodes. A gate voltage V_g is applied to the third electrode in the upper left corner to vary the electrostatic potential of the nanotube. (b) Current–voltage curves of nanotubes for different V_g-values (A: 88.2 mV, B: 104.1 mV and C: 120.0 mV). More I–V curves are shown in the inset with V_g ranging from 50 mV (bottom curve) to 136 mV (top curve). (Reproduced from reference [53].)

An interesting transport experiment was performed by Frank *et al* [135]. MWNTs were dipped into liquid metal with the help of a scanning probe microscope tip and the conductance was measured simultaneously. Figures 8(a) and 8(b) show the nanotube contact used in the measurements. The nanotubes were straight with lengths of 1 to 10 μm. As the nanotubes were dipped into the liquid metal one by one, the conductance increased in steps of $(2e^2/h)$ as shown in figure 8(c). Each step corresponds to an additional nanotube coming into contact with liquid metal. The electronic transport is found to be ballistic, since the step heights do not depend on the different lengths of nanotubes coming into contact with the metal.

On the theory side, different techniques are used to calculate quantum effects on the conductance of nanotubes [94, 96, 97, 99, 136–139]. These techniques are based on linear response theory and use the Landauer formalism. Tian and Datta [136] studied the tip–nanotube–substrate system in STM and investigated the Aharonov–Bohm effect in nanotubes
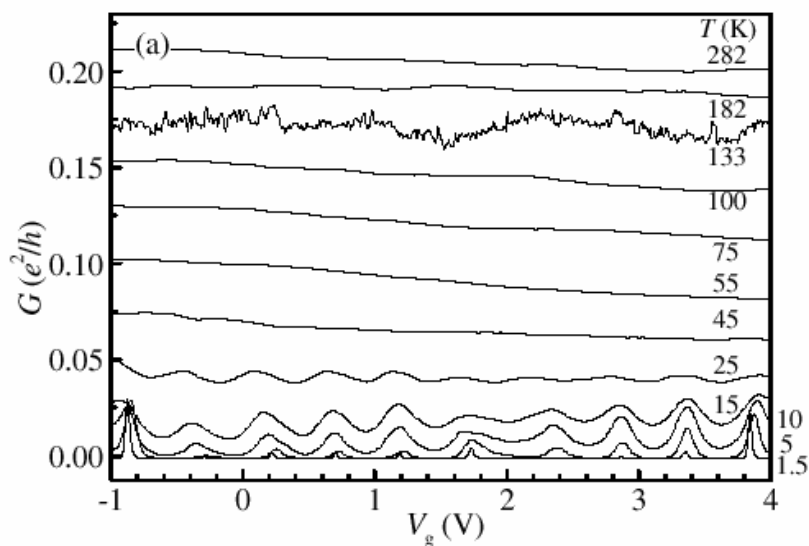
Figure 7. Variation of the conductance with the gate voltage at temperatures from 1.5 K to 282 K for a nanorope with metallic tubes. (Reproduced from reference [128].)
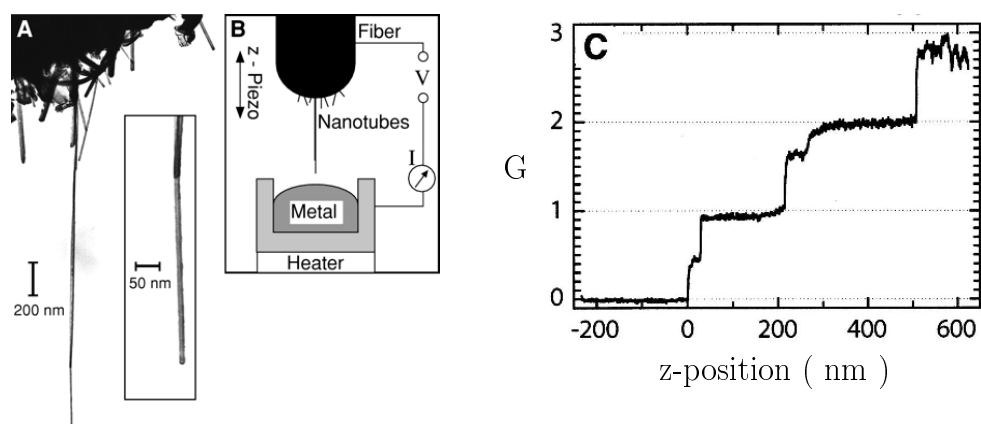

Figure 8. (A) A transmission electron micrograph (TEM) image of the end of a nanotube fibre which consists of carbon nanotubes and small graphitic particles. (B) A schematic diagram of the experimental set-up. Nanotubes are lowered under SPM control to a liquid metal surface. (C) Variation of conductance with nanotube fibre position. Plateaus are observed corresponding to additional nanotubes coming into contact with the liquid metal. (Reproduced from reference [135].)

using the Landauer formula. They treated the transmission coefficient using a semiclassical approach. Saito *et al* [137] studied tunnelling conductance of nanotube junctions which are joined by a connecting region with a pentagon–heptagon pair. They used a method for directly calculating the current density. Tamura and Tsukada [138] used effective-mass theory with envelope functions for similar junctions. Choi and Ihm [94] presented an *ab initio* pseudopotential method with a transfer-matrix approach and studied nanotubes with pentagon–heptagon pair defects. Among these methods, Green's function methods [96, 97, 99] are

found to be the most effective and hence are widely used for nanotubes with local basis sets. Chico *et al* [97] studied nanotubes having vacancies and other defects by using a Green's function technique with a surface Green's function matching method [98]. Carbon nanotubes with disorder were studied by Anantram and Govindan [99] using a similar Green's function technique with an efficient numerical procedure. Recently, Nardelli [96] presented an approach using a surface Green's function matching method. Iterative calculations of transfer matrices are combined with the Landauer formula to calculate the conductance. In these techniques, electronic structures of nanotubes are derived from the π-orbital tight-binding model.

4.3. Nanotube junctions and devices

Current trends in microelectronics are to produce smaller and faster devices. Owing to the novel and unusual mechanical and electronic properties, carbon nanotubes appear to be potential candidates for meeting the demands of nanotechnologies. There are already nanodevices which use nanotubes. Single-electron transistors were produced [53, 54] by using metallic tubes; the devices formed therefrom have operated at low temperatures. Tans *et al* [140] demonstrated a field-effect transistor that consists of a semiconductor nanotube and operates at room temperature. The nanotube placed on two metal electrodes and a Si substrate which is covered with SiO_2 is used as a back-gate. The nanotube is switched from a conducting to an insulating state by applying a gate voltage.

One approach used in making a nanodevice was based on the fact that the defects in a nanotube can form an intermolecular junction from an individual tube [137, 141, 142]. It was shown that topological defects like pentagon–heptagon pair defects can change the helicity and hence the electronic structure of the nanotube. This raises the possibility of fabricating metal–metal (M–M), metal–semiconductor (M–S) and semiconductor–semiconductor (S–S) junctions on a single nanotube. In figure 9(a), the atomic structure of a M–S junction is shown [141]. An (8, 0) tube (semiconductor) is joined to a (7, 1) tube (metal) with a pentagon–hexagon defect (highlighted in grey). The local density of states (LDOS) based on a π-orbital tight-binding model is presented in figure 9(b). The LDOS is distorted close to the interface, but recovers the DOS of a perfect tube away from the interface on both sides. There is a conductance gap in M–S and S–S junctions [143] and diode-like behaviour can be achieved. However, in M–M junctions, the conductance was found to depend on the arrangement of the defects [97]. The junction is insulating for symmetric arrangement, but conducting for asymmetric arrangement. Kink structures which consist of such defects have been observed experimentally [143–145]. Even electronic transport measurements were reported, by Yao *et al* [146], on nanotubes with M–M and M–S junctions. They found that a M–S junction behaves like a rectifying diode with non-linear transport characteristics and the conductance of the M–M junction was suppressed. Other intermolecular junctions include nanotube–silicon nanowire junctions [147] and Y-junctions [148] which exhibit rectification.

So far we have discussed nanotube junctions and devices that used individual nanotubes. Two or more nanotubes can form nanoscale junctions with unique properties [149]. A simple intermolecular nanotube junction can be formed by bringing two tube ends together. Figure 10(a) illustrates such a junction with two semi-infinite (10, 10) tubes in parallel and pointing in opposite directions. Buldum and Lu [149] showed that these junctions have high conductance values and exhibit negative differential resistance behaviour. Interference of electron waves reflected and transmitted at the tube ends gives rise to the resonances in conductance shown in figure 10(b). The current–voltage characteristics of this junction presented in figure 10(c) show a negative differential resistance effect, which may have applications in high-speed switching, memory and amplification devices.
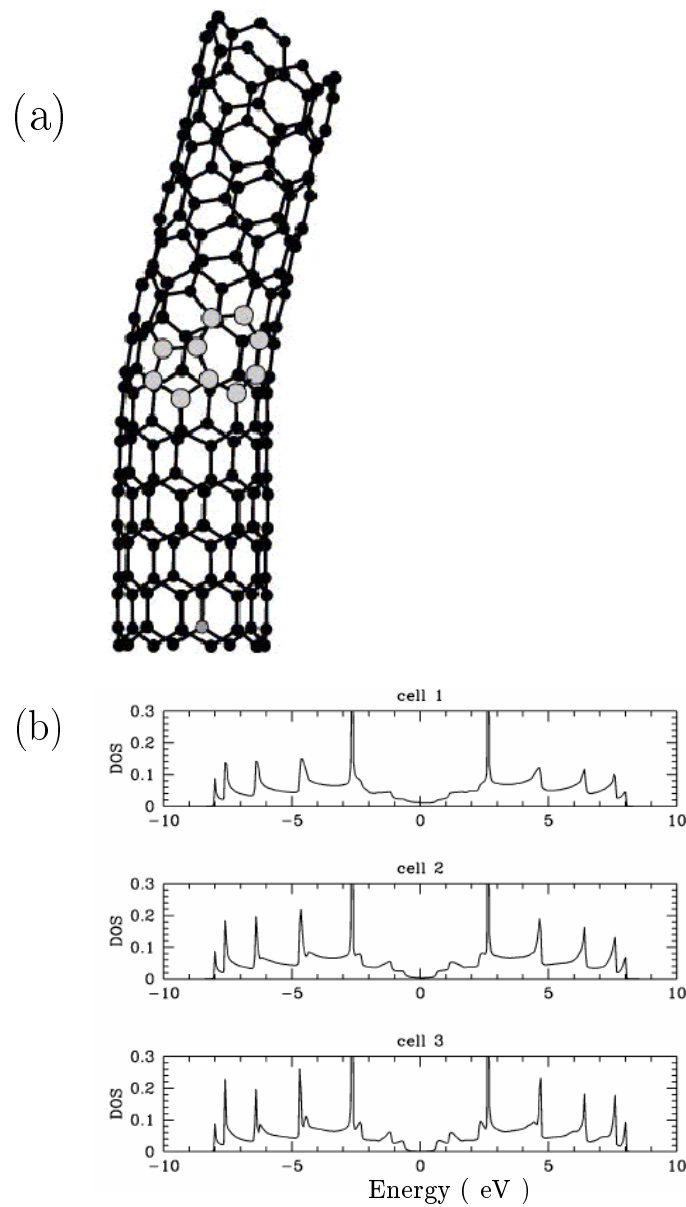
Figure 9. (a) Atomic structure of a semiconductor–metal junction ((8, 0)–(7, 1)) with a pentagon–hexagon pair defect. Grey balls denote the atoms forming the defect. (b) The local density of states (LDOS) at cells 1, 2 and 3. Cell 3 is on the (8, 0) side of the tube and cell 1 is at the interface. (Reproduced from reference [141].)

A four-terminal junction can be constructed by placing one nanotube perpendicular to another and forming a cross-junction (figure 11(a)). Fuhrer *et al* [150] reported electronic transport measurements of cross-junctions and presented M–M, M–S and S–S four-terminal devices. The M–M and S–S junctions had high conductance values ($\sim 0.1 e^2/h$) and the M–S junction formed a rectifying Schottky barrier. Buldum and Lu [149] found that the
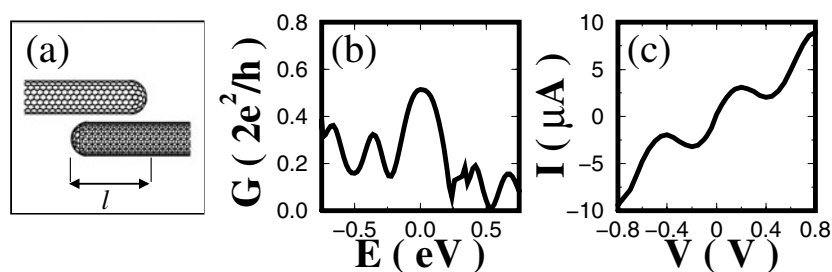
Figure 10. (a) An intermolecular nanotube junction formed by bringing two semi-infinite (10, 10) tubes together. l is the contact length. (b) The conductance, G, of a (10, 10)–(10, 10) junction as a function of energy, E, for $l = 64$ Å. Interference of electron waves yields resonances in conductance. (c) Current–voltage characteristics of a (10, 10)–(10, 10) junction at $l = 46$ Å. (Reproduced from reference [149].)
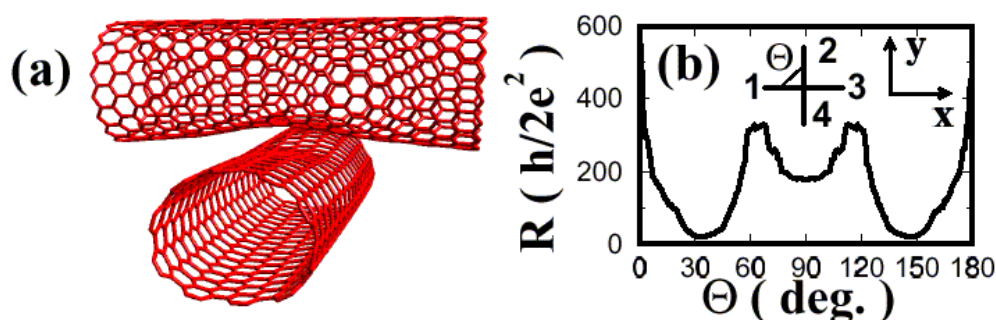

Figure 11. (a) A four-terminal cross-junction with two nanotubes perpendicular to each other. (b) The resistance of an (18, 0)–(10, 10) junction as a function of tube rotation. The rotation angle, Θ, and terminal indices are shown in the inset. The tube which is labelled by 2 and 4 is rotated by Θ. The contact region structure is commensurate at $\Theta = 30, 90, 150°$. (Reproduced from reference [149].)

conductance of such intermolecular junctions strongly depends on the atomic structure in the contact region. Conductance between the tubes was found to be high when the junction region structure was commensurate and conductance was low when the junction was incommensurate. Figure 11(b) shows the variation of the resistance with the rotation of one of the tubes. The junction structure is commensurate at angles $30°$, $90°$ and $150°$, and hence the resistance values are lower. Similar variation of the resistance with the atomic structure in the contact region is observed in nanotube–surface systems [151]. This significant variation of transport properties with atomic scale registry was found also in mechanical/frictional properties of nanotubes [152, 153]. Recently, Rueckes *et al* [154] introduced a random-access memory device for molecular computing which is based on cross-junctions. They showed that cross-junctions can have bistable, electrostatically switchable on/off states and an array of such junctions can be used as an integrated memory device.

5. Thermal conductance

The steady-state heat current density (i.e. heat transfer per unit time per unit cross section) in a diffused regime in one dimension is given [16, 17] by $j_H = -K \, dT/dx$. Because of the random nature of the transport, the heat current involves the temperature gradient and the

thermal conductivity K. Let us now consider a quasi-one-dimensional (1D) constriction or a nanowire connecting two reservoirs (i.e. left reservoir L and right reservoir R). The length and width of the constriction are l and w, respectively. The energy can be transferred from L to R by means of phonons and electrons, which obey different statistics. The analysis of electrical and thermal conduction in ballistic and mesoscopic systems has used Landauer's celebrated theory of transport [19]. In dielectric wires the energy is transported only by phonons. In metallic wires, the energy transported by electrons dominates over that transported by phonons. We discuss the electronic and phononic thermal transport in separate subsections below.

5.1. Quantum of electronic thermal conductance

Sophisticated and mathematically precise treatments of electronic heat transfer can already be found in various textbooks [16, 17]. The emphasis here is primarily on providing a more intuitive understanding of the thermal conductance quantization, a phenomenon not encountered in our daily-life experiences and hence perhaps difficult to grasp. Here we explain how the quantum of thermal conductance can be obtained (within a numerical factor) as a consequence of Heisenberg's uncertainty principle [155].

When the width of the constriction is in the range of the Fermi wavelength (i.e. $w \sim \lambda_F$), the transverse motion of electrons confined to w becomes quantized. The finite level spacing of the quantized electronic states reverberates into the ballistic electron transport, and gives rise to resolvable quantum features in the variation of electrical and thermal conductance. If the energy propagates ballistically without deflection and the net particle current (or electrical current I) is zero, then the heat current (or the flux of electronic thermal energy) from L to R, $\mathcal{J}_e$, depends only on the temperature difference between the two reservoirs [156, 157], $\Delta T = T_L - T_R$. The thermal conductance $\mathcal{K}_e$ is the ratio of the total electronic heat current to the temperature difference:

$$\mathcal{K}_e = \frac{\mathcal{J}_e}{\Delta T}. \tag{15}$$

It is related to the thermal conductivity K_e through the relation $\mathcal{K}_e = K_e w / l$ for a strip. For a nanowire having a finite cross section, w should be replaced by the cross sectional area.

We are interested in obtaining the quantum analogue of $\mathcal{K}_e$ in equation (15) when w and l are below certain characteristic lengths. When w becomes small, the electronic energy level spectrum becomes discrete. A natural characteristic length for w is the Fermi wavelength λ_F, since the number of transverse occupied states, N, in a constriction is $2w/\lambda_F$. The characteristic length along the propagation direction is the electron mean free path l_e. If $T_L > T_R$ and $l < l_e$, the carriers moving between L and R through the nanowire will transfer energy. With w in the range of λ_F and l in the range of l_e, we are in a nanodomain and expect the quantum features to set in for $\mathcal{K}_e$, which we now demonstrate using Heisenberg's uncertainty principle. We start by recalling that the total heat current $\mathcal{J}_e$ is

$$\mathcal{J}_e = \frac{\mathrm{d}E}{\mathrm{d}t}. \tag{16}$$

In the extreme quantum limit, when a single carrier moves from L to R across the wire, an energy $k_B T_L$ flows across the junction. In this limit, one can also assume the transit time to lie in the range set by Heisenberg's uncertainty principle ($\mathrm{d}t \sim \Delta t$). But to maintain the $I = 0$ condition, one carrier must also flow from R to L across the nanowire. Hence under ballistic conditions $\mathrm{d}E = k_B \Delta T$ and

$$\mathcal{J}_e = \frac{k_B \Delta T}{\Delta t}. \tag{17}$$

Only electrons within the thermal energy of the Fermi level can propagate across the nanowire. Assuming the uncertainty in energy to be of the order of the thermal spread, $\Delta E \sim k_B T$, where $T = (T_L + T_R)/2$, and combining equation (15) and (17), one gets

$$\mathcal{K}_e \sim \frac{k_B^2 T}{\Delta E \, \Delta t}. \tag{18}$$

Next, invoking Heisenberg's uncertainty principle as an *ansatz*, $\Delta E \, \Delta t \sim h$, equation (18) becomes

$$\mathcal{K}_e \sim 2 \frac{k_B^2}{h} T \tag{19}$$

where the factor of two arises from the spin degeneracy. It should be noted that the uncertainty principle is really an inequality, $\Delta E \, \Delta t \geqslant \hbar/2$. Therefore our intuitively obtained value in equation (19) may well be off by factors of 2, or π, etc. But it traces the origin of the quantum of thermal conductance to a fundamental principle of quantum mechanics, namely the Heisenberg uncertainty principle. The precise expression for the quantum of thermal conductance is [156]

$$\mathcal{K}_0 = \frac{\pi^2}{3} \frac{k_B^2}{h} T \tag{20}$$

which is equal to $\sim 10^{-12} T$ W K^{-1}. If we now recall the electrical conductance in the extreme quantum limit, i.e. the quantum of conductance $G = 2e^2/h$, and construct the ratio $\mathcal{K}_e/G$ we get

$$W = \frac{\mathcal{K}_e}{G} = \frac{k_B^2 T}{e^2}. \tag{21}$$

This, apart from a numerical factor, is the statement of the Wiedemann–Franz law [16, 158]. It is fascinating that it holds equally well in the quantum domain.

5.2. The quantum of phononic thermal conductance

Effects similar to those in the ballistic electrical conduction are expected to occur in the heat conduction *via phonons*. An atomic wire (or in general a nano-object) has a discrete vibrational frequency spectrum with finite spacing $\Delta\omega_i = \omega_{i+1} - \omega_i$, which is determined by the atomic configuration and size of the nano-object. Once such a wire is coupled to two reservoirs, collective vibrational modes (phonons) which involve the coherent vibrations of the atoms in the wire and reservoirs can be developed, leading to the process of ballistic thermal conduction. The phononic thermal conductance, $\mathcal{K}_p$, depends on the number of channels available and hence it is expected to increase by discrete amounts each time a new ballistic channel is included in the heat transfer. Each vibrational mode contributes to the heat transfer, but its contribution is weighted by Planck's distribution $n(\omega, T)$.

The answer to the fundamental question of whether the phononic thermal conductance has an upper limit has been sought in recent theoretical studies [61–63]. These studies involved the phononic heat transfer between two heat reservoirs (L and R) through a long dielectric bridge or atomic chain (C). Each reservoir has a continuous density of phonon states $g_i^{L,R}(\omega)$ for a given branch i, and the connecting chain has discrete phonon states, $g^C(\omega)$. The reservoirs are maintained at constant temperature, T_L and T_R, with $\Delta T = T_L - T_R$, so the heat transport is realized in the steady state (see figure 12). Furthermore, the transmission process is assumed to be perfect with the transmission coefficient $\mathcal{T} = 1$. By using a Landauer-type approach [19, 61, 62] or a phenomenological Hamiltonian approach and rate theory [63], and
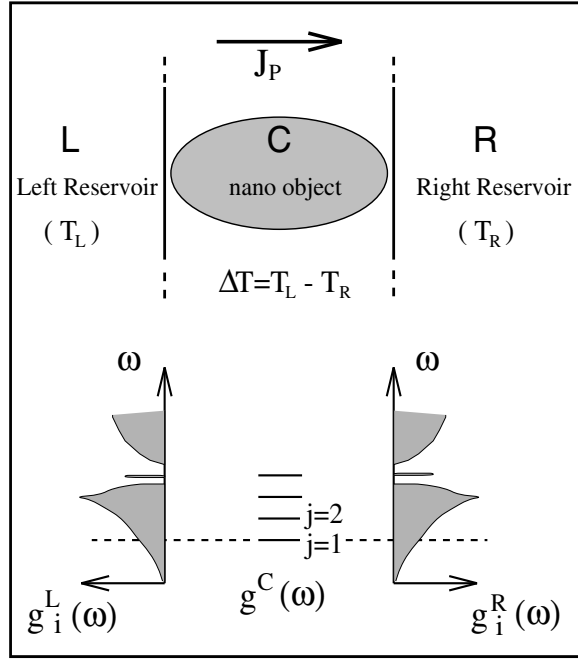
Figure 12. A schematic diagram of the quantum heat transfer through a nano-object between the left (L) and right (R) electrodes. The densities of phonon states of the left electrode $g_i^L(\omega)$, right electrode $g_i^R(\omega)$ and nano-object $g^C(\omega)$ are also shown schematically. Resonant modes are indicatd by a dotted line.

assuming T_L and T_R are small and ΔT is much smaller than T_L and T_R, the following universal expression:

$$\mathcal{K}_p = \sum_i \frac{\pi^2 k_B^2}{3h} T \tag{22}$$

for the ballistic thermal conductance through a uniform chain is found. Here the summation is over the branches of the phonon dispersion curves. According to this result the ballistic conductance of each branch i of the uniform and harmonic atomic chain is limited by the value $\mathcal{K}_0 = \pi^2 k_B^2 T/3h$. It is independent of any material parameter, and is linearly dependent on $T = (T_L + T_R)/2$. The total thermal conductance becomes $\mathcal{K}_p = \mathcal{N}\mathcal{K}_0$, where $\mathcal{N}$ is the total number of phonon branches. For an ideal 1D atomic chain, $\mathcal{N} = 3$, if the transverse vibrations are allowed.

For a homogeneous wire that has a large cross section, more subbands can be present due to the transverse confinement of the vibrational motions in the direction perpendicular to the heat propagation. In this case, the ballistic thermal conductance of a branch with $\Omega_{i,min} \neq 0$ is smaller than $\mathcal{K}_0$ due to the finite frequency of a subband through the occupancy of Planck's distribution. One expects each subband in the wire having $\Omega_{i,min} \neq 0$ to lead to a jump in $\mathcal{K}_p$ exactly as in the electrical conduction. However, the steps are smeared out and their amplitudes decrease exponentially with increasing $\Omega_{i,min}$ at finite temperature. An important difference between the electrical and thermal conductance is that all the modes of a given branch i contribute to $\mathcal{K}_p$, whereas the quantum ballistic electrical conduction G is governed by the Fermi–Dirac distribution.

5.3. Quantum effects in phononic thermal conductance

In view of the above discussion, one can ask as to how the discrete vibrational frequency spectrum is reflected in the thermal conductance $\mathcal{K}_p$. Also, what quantum features similar to those of ballistic electron conduction would be involved in the phononic energy transfer through a small molecule or nanowire? Satisfactory answers to these questions are essential for several physical events and chemical processes in biology, molecular electronics and nanoscience. Here, we discuss various quantum effects in the phononic energy transfer through the nano-object represented by a finite monatomic chain. This discussion is based on the formalism developed by Özpineci and Ciraci [65] using Keldysh's theory of the non-equilibrium process [159].

The physical system of interest is shown schematically as an inset in figure 13(a). Two reservoirs (L and R) with temperatures T_L and T_R are described by the vibrational Hamiltonians $\mathcal{H}_L$ and $\mathcal{H}_R$, respectively. L and R are connected by a dielectric chain of N atoms, that is described by the following Hamiltonian:

$$\mathcal{H}_C = \sum_{i=1}^{N} \frac{p_i^2}{2M} + \sum_{i=1}^{N-1} \frac{k}{2}(x_i - x_{i+1})^2 + \frac{k}{2}x_1^2 + \frac{k}{2}x_N^2 \tag{23}$$

where p_i and x_i are the momentum and displacement of the ith atom, respectively. In this Hamiltonian the couplings to L and R are not considered; only the harmonic interactions with the nearest-neighbour coupling k in the chain are taken into account. The end atoms ($i = 1$ and $i = N$) are connected to the reservoirs. The couplings of the chain to L and R are described, to the lowest order, by the Hamiltonian

$$\mathcal{H}_{int} = A_L u_L x_1 + A_R u_R x_N \tag{24}$$

where the $u_{L,R}$ stand for the lateral displacements of reservoir atoms which are coupled to the chain. A_L and A_R are coupling parameters. Only one atom from each reservoir is assumed to interact with the chain, and only the longitudinal mode is considered. This model, though simple, is capable of revealing the underlying physics of phononic energy transfer through atomic wires as long as the level spacing, $\Delta\omega$, is sufficiently large. The details of the formalism and definitions of the Green's functions can be found in references [159, 160].

We start with the expectation value of the current through this atomic wire which has been cast in the Landauer form [19]

$$J_p = \frac{1}{2\pi} \sum_{ml} \int d\omega \, \hbar\omega[n^L(\omega, T_L) - n^R(\omega, T_R)]\mathcal{T}_{ml}(\omega). \tag{25}$$

Here $n^L(\omega, T)$ and $n^R(\omega, T)$ are Planck's distribution functions for L and R, respectively. $\mathcal{T}_{ml}(\omega)$ stands for the transmission coefficient for a phonon of frequency ω from the mth branch of L to the lth branch of R, and is expressed as

$$\mathcal{T}_{ml}(\omega) = (2\pi)^2 \left(\frac{A_L A_R}{\hbar^2}\right)^2 g_m^L(\omega) g_l^R(\omega) \det \mathcal{G}_{1N}(\omega) \frac{\hbar}{2M_L\omega} \frac{\hbar}{2M_R\omega} \tag{26}$$

where $g_m^{L\,(R)}$ and $M_{L\,(R)}$ are the phonon density of states corresponding to mth branch and mass of atoms of L (R), respectively. Note that here $\mathcal{G}^a$ and $\mathcal{G}^r$ are advanced and retarded Green's functions, respectively, and $\det \mathcal{G}_{1N} = \mathcal{G}_{1N}^a \mathcal{G}_{1N}^r$. Finally, the heat current from L to R in the steady state is given by

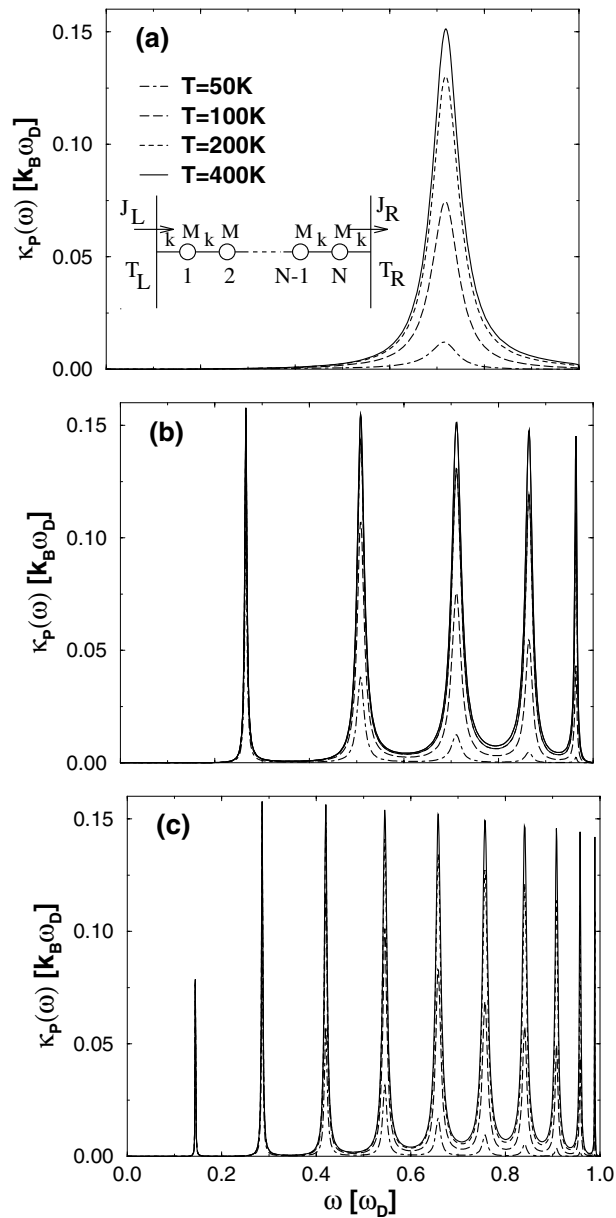$$J_p(T_L, T_R) = \int_0^1 dx \, J_p(x\omega_D, T_L, T_R)$$

Figure 13. Variation of the thermal conductance density $\mathcal{K}_p(\omega)$ with temperature T, and number of atoms in the chain N, for $\sqrt{k/M} = 0.5\omega_D$. The inset shows the model used for the phononic energy transfer. The chain consists of N atoms; each atom of mass M is undergoing a harmonic interaction with nearest-neighbour coupling k. (a) $N = 1$; (b) $N = 5$; (c) $N = 10$. (Reproduced from reference [65].)

where $J_p(\omega, T)$ is the heat current density at frequency ω. Then the heat conductance density at T is defined by

$$\mathcal{K}_p(\omega, T) = \lim_{\Delta T \to 0} J_p(\omega, T + \Delta T, T)/\Delta T.$$

The total conductance $\mathcal{K}_p$ is calculated from the integral of the conductance density $\mathcal{K}_p(\omega, T)$ over all the frequencies up to ω_D, i.e.

$$\mathcal{K}_p = \int_0^1 \mathrm{d}x \; \mathcal{K}_p(x\omega_D, T).$$

Note that $\mathcal{K}_p$ is independent of ω; it increases first with increasing T and eventually saturates at a value depending on the parameters of the heat-conducting system.

Numerical results for the above formalism of heat transfer were obtained [65] assuming that the two reservoirs are identical, and their phonon densities of states are treated within the Debye approximation, and also $\hbar\omega_D^R = \hbar\omega_D^L = \hbar\omega_D = 37.6$ meV; $M_L = M_R = 56$ amu, $M = 28$ amu; $A_L = A_R = -19$ J m^{-2}. Figures 13(a)–13(c) show the variation of the conductance density, $\mathcal{K}_p(\omega)$, with temperature and number of atoms in the chain, N. $\mathcal{K}_p(\omega)$ appears as Lorentzian-type resonances at the eigenfrequencies of the chain, ω_i. The heights of the resonances depend on T and ω_i. The higher the ω_i and the lower the T, the lower the height of the resonances. This behaviour originates from Planck's distribution function. At sufficiently high temperature, the heights of the resonances become independent of N. However, $\mathcal{K}_p(\omega)$ resonances become narrow as N becomes large. This behaviour can be understood in terms of the weakening of the coupling of each mode which is proportional to $1/\sqrt{N+1}$.

Owing to the coupling to the reservoirs, the total conductance $\mathcal{K}_p$ depends on the material parameters k and M through $\Omega = \sqrt{k/M}$. As Ω increases, the eigenfrequencies of the modes, ω_i, increase; starting from the highest one, they cross the Debye frequency, ω_D, one by one. Each ω_i that rises above ω_D, and thus gets out of the range of $g^{L\,(R)}(\omega)$, ceases to contribute to the thermal conductance. In this way, a channel closes and $\mathcal{K}_p$ decreases suddenly, leading to a step structure in the variation of $\mathcal{K}_p$ with Ω. The larger the level spacing $\Delta\omega_i$, the longer the plateau. Since all $\omega_i < \omega_D$ contribute to the thermal conduction at high temperature, one can obtain a multiple-step structure for large N ($N > 3$). Also the step structure becomes pronounced at high temperature. This situation is contrary to the electronic counterpart: ballistic electron conductance, where the steps become less pronounced due to the smearing of the Fermi distribution at high temperature [24].

The variation of the total conductance with temperature is shown in figure 14 for a particular chain parameter, Ω, and $N = 5$. In the high-temperature limit, $\left[n^L(\omega, T_L) - n^R(\omega, T_R)\right]$ in equation (25) can be approximated by $k_B \Delta T/\hbar\omega$. Then $\mathcal{K}_p$ saturates at a value that depends on the couplings A_R and A_L, as well as on the density of states of the reservoirs, L and R. At low temperature, the discrete vibrational spectrum affects the variation of $\mathcal{K}_p$ with temperature if the wire has a vibrational mode in the range of $k_B T$. This situation is examined by considering a 'soft' chain with $\Omega = \omega_D/100$. As shown by the inset, the calculated $\mathcal{K}_p$ versus T jumps when the second vibrational mode begins to contribute to the conduction. Clearly, the discrete vibrational spectrum of a 'soft' chain is reflected in the thermal conductance by giving rise to a sudden increase at low temperature.

The variation of the total conductance $\mathcal{K}_p$ with N for different coupling constants (i.e. for different Ω) can now be addressed. For a 'soft' chain with $\Omega = \omega_D/2$, $\mathcal{K}_p$ is independent of N at high temperature, since all modes have frequency $\omega_i < \omega_D$ and hence all modes contribute to the conduction. However, for a 'stiff' chain with $\Omega = \omega_D$, $\mathcal{K}_p$ fluctuates with N since ω_D falls in the spectrum of the chain $g^C(\omega)$ and thus the number of contributing modes changes with N. Fluctuations decrease with increasing N and decreasing T. For $N \leqslant 2$, $\mathcal{K}_p$ is slightly decreased even for the soft chain, since the conductance density $\mathcal{K}_p(\omega)$ is broadened and its contribution to the conductance decreases when its tail exceeds ω_D. This situation is similar to that found by Lang [34], where the electrical conductance through a single atom
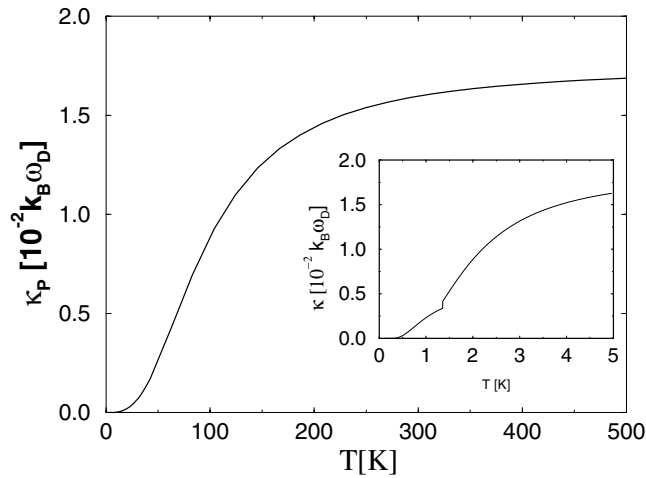
Figure 14. The total conductance $\mathcal{K}_p$ versus temperature for $N = 5$ and $\sqrt{k/M} = 0.5\omega_D$. The behaviour of $\mathcal{K}_p$ at low temperature is shown by the inset. (Reproduced from reference [65].)

was found to be smaller than that of a chain containing 2–4 atoms. In summary, if all the eigenfrequencies, ω_i, are smaller than ω_D, $\mathcal{K}_p$ becomes independent of N at high temperature. Note that the conductance channels increase with increasing number of modes and hence with increasing N. However, this does not mean that the conductance will increase with increasing N, since the coupling to the reservoirs will be weakened with increasing N. Moreover, $\mathcal{K}_p$ normally decreases with increasing number of atoms in the chain due to the increasing chance of scattering.

6. Conclusions

The quantization of states in the nano-objects yields finite energy level spacings. The relative energy positions and the occupancy of these states are closely related to the atomic configuration. When such a nano-object connects two reservoirs, the electrons (phonons) pass through from one reservoir to the other under finite bias (finite temperature difference). The finite level spacing and the relative energy positions of these states are reflected in the transport properties, in particular the conductance. In the electrical conductance of nanowires, several current-transporting states or channels contribute to the conductance when the cross section of the metallic wire includes several atoms. The sudden changes in the variation of the conductance with stretching are shown to be related to sudden and discontinuous changes in the cross section of the wire.

Molecular dynamics calculations carried out using an empirical potential showed that the elongation and yielding mechanisms of a nanowire under uniaxial tensile force depend on its size, atomic structure and temperature. The wires with small cross section yield either by order–disorder structural transformation or by a single-atomic process. Shortly before the break, the structure is transformed to form a bundle of atomic chains or a monatomic atomic chain at the neck.

The electronic conductance of a metallic SWNT is dependent on the character of the contacts to the electrodes. It can provide ballistic conductance close to $2(2e^2/h)$ with good contacts, and transmit high current density. With their novel transport properties, carbon nanotubes will be a subject of interest in quantum transport studies for the next decade.

The quantum of conductance for electric and thermal transport by electrons is obtained within a numerical factor upon invoking Heisenberg's uncertainty principle as an *ansatz*. Using the quanta of thermal and electrical conductance it has been shown that the Wiedemann–Franz law holds for nanostructures.

The ballistic thermal conductance of each branch of a uniform wire or chain is limited by a universal value that is independent of any material parameter and is linearly dependent on the temperature. The finite level spacings of the eigenfrequencies of an atomic chain (or nano-object) are reflected in the variation of the phononic thermal conductance. Resonance structure is revealed in the variation of the conductance density. One channel of heat conduction is closed as soon as an eigenfrequency of the chain comes out of the range of the quasi-continuous phonon frequency (or density of states) of the reservoirs. This gives rise to an effect analogous to the formation of plateaus observed in the electrical conductance of a quasi-2D constriction with variable width or of a stretching metal wire.

The interest in nanostructures from the perspective of nanotechnology is now well established. It will not be long before we see fascinating applications in fields ranging from genetics to quantum computing.

References

[1] Esaki L (ed) 1991 *Highlights in Condensed Matter and Future Prospects (Nato ASI vol 285)* (New York: Plenum)
  Gimzewski J K and Welland M E (ed) 1995 *Ultimate Limits of Fabrication and Measurements (Nato ASI vol 292)* (Dordrecht: Kluwer)
  Serena P A and Garcia N (ed) 1997 *Nanowires (Nato ASI)* (Dordrecht: Kluwer)
[2] Gimzewski J K and Möller R 1987 *Phys. Rev.* B **41** 2763
[3] Agraït N, Rodrigo J G and Vieira S 1993 *Phys. Rev.* B **47** 12 345
[4] Pascual J I, Méndez J, Gómez-Herrero J, Baró A M, Garcia N and Binh V T 1993 *Phys. Rev. Lett.* **71** 1852
[5] Olesen L, Laegsgaard E, Stensgaard I, Besenbacher F, Schiøtz J, Stoltze P, Jacobsen K W and Nørskov J K 1994 *Phys. Rev. Lett.* **72** 2251
[6] Krans J M, Müller C J, Yanson I K, Gowarent T C M, Hesper R and van Ruitenbeek J M 1994 *Phys. Rev.* B **50** 14 721
  Krans J M *et al* 1995 *Nature* **375** 767
[7] Pascual J I, Méndez J, Gómez-Herrero J, Baró A M, Garcia N, Landman U, Luedtke W D, Bogachek E N and Cheng H P 1995 *Science* **267** 1793
[8] Yazdani A, Eigler D M and Lang N D 1996 *Science* **272** 1921
[9] Ohnishi H, Kondo Y and Takayanagi K 1998 *Nature* **395** 780
[10] Yanson A I, Bolliger G R, van der Brom H E, Agraït N and van Ruitenbeek J M 1998 *Nature* **395** 783
[11] Binnig G, Rohrer H, Gerber Ch and Weibel E 1982 *Phys. Rev. Lett.* **49** 57
  Binnig G, Quate C and Gerber Ch 1986 *Phys. Rev. Lett.* **56** 930
[12] Agraït N, Rubio G and Vieira S 1995 *Phys. Rev. Lett.* **74** 3995
  Rubio G, Agraït N and Vieira S 1996 *Phys. Rev. Lett.* **76** 2302
[13] Stalder A and Dürig U 1996 *Appl. Phys. Lett.* **68** 637
[14] van Wees B J, van Houten J, Beenakker C W J, Williams J G, Kouwenhoven L P, van der Marel D and Foxon C T 1988 *Phys. Rev. Lett.* **60** 848
[15] Wharam D A, Thornton T J, Newbury R, Pepper M, Ritchie H and Jones G A C 1988 *J. Phys. C: Solid State Phys.* **21** L209
[16] Kittel C 1996 *Introduction to Solid State Physics* (New York: Wiley) p 166
[17] Ziman J M 1965 *Theory of Solids* (Cambridge: Cambridge University Press) p 196
[18] Batra I P 1998 *Surf. Sci.* **395** 43
[19] Landauer R 1957 *IBM J. Res. Dev.* **1** 223
  Landauer R 1970 *Phil. Mag.* **21** 863
  Landauer R 1989 *J. Phys.: Condens. Matter* **1** 8099
[20] Lang N D 1987 *Phys. Rev.* B **36** 8173
[21] Ferrer J, Rodero A M and Flores F F 1988 *Phys. Rev.* B **38** 10 113
[22] Ciraci S and Tekman E 1989 *Phys. Rev.* B **40** R11 969

[23] Ciraci S 1990 *Tip–Surface Interactions in Scanning Tunnelling Microscopy and Related Methods* vol 184, ed R J Behm, N Garcia and H Rohrer (Dordrecht: Kluwer Academic) p 113

[24] Tekman E and Ciraci S 1991 *Phys. Rev.* B **43** 7145

[25] Todorov T N and Sutton A P 1993 *Phys. Rev. Lett.* **70** 2138

[26] Torres J A, Pascual J and Sáenz I 1994 *Phys. Rev.* B **49** 16 581

[27] Bratkovsky A M, Sutton A P and Todorov T N 1995 *Phys. Rev.* B **52** 5036

[28] Lang N D 1995 *Phys. Rev.* B **52** 5335

[29] Costa-Krämer J L, Garcia N, Garcia-Mochales P and Serena P A 1995 *Surf. Sci.* **342** L1144

[30] Torres J A and Sáenz J J 1996 *Phys. Rev. Lett.* **77** 2245

[31] Müller C J, Krans J M, Todorov T N and Reed M A 1996 *Phys. Rev* B **53** 1022

[32] Todorov T N and Sutton A P 1996 *Phys. Rev.* B **54** R14 234
     Todorov T N and Sutton A P 1996 *Phys. Rev.* B **54** 2138

[33] Brandbyge M, Jacobsen K W and Nørskov J K 1995 *Phys. Rev.* B **52** 8499
     Brandbyge M, Jacobsen K W and Nørskov J K 1997 *Phys. Rev.* B **55** 2637
     Brandbyge M, Jacobsen K W and Nørskov J K 1997 *Phys. Rev.* B **56** 14 956

[34] Lang N D 1997 *Phys. Rev. Lett.* **79** 1357

[35] Mehrez H and Ciraci S 1997 *Optical Spectroscopy of Low Dimensional Semiconductors* vol 344, ed G Abstreiter, A Aydinli and J P Leburton (New York: Kluwer) p 213

[36] Mehrez H and Ciraci S 1997 *Phys. Rev.* B **56** 12 632

[37] Mehrez H, Ciraci S, Buldum A and Batra I P 1997 *Phys. Rev.* B **55** R1981

[38] Mehrez H and Ciraci S 1998 *Phys. Rev.* B **58** 9674

[39] Landman U, Luedtke W D, Salisbury B E and Whetten R L 1996 *Phys. Rev. Lett.* **77** 1362
     Yannouleas C and Landman U 1997 *J. Phys. Chem.* B **101** 5780

[40] Bogachek E N, Scherbakov A G and Landman U 1997 *Phys. Rev.* B **56** 1065

[41] Levy Y, Martin-Rodero A and Flores F 1997 *Phys. Rev.* B **56** 10 369

[42] Wan C C, Mozos J L, Taraschi G, Wang J and Guo H 1997 *Appl. Phys. Lett.* **71** 419

[43] Cuevas J C, Levy Y and Martin-Rodero A 1998 *Phys. Rev. Lett.* **80** 1066

[44] Iijima S 1991 *Nature* **354** 56
     Iijima S and Ishibashi T 1993 *Nature* **363** 603

[45] Dresselhaus M S, Dresselhaus G and Ecklund P C 1996 *Science of Fullerenes and Carbon Nanotubes* (San Diego, CA: Academic)

[46] Ebbesen T (ed) 1997 *Carbon Nanotubes: Preparation and Properties* (Boca Raton, FL: Chemical Rubber Company Press)

[47] Saito R, Dresselhaus G and Dresselhaus M S 1998 *Physical Properties of Carbon Nanotubes* (London: Imperial College Press)

[48] Lu J P 1997 *Phys. Rev. Lett.* **79** 1297

[49] Falvo M R *et al* 1997 *Nature* **389** 582

[50] Wildöer J W G, Venema L C, Rinzler A G, Smalley R E and Dekker C 1998 *Nature* **391** 59

[51] Odom T W, Huang J L, Kim P and Lieber C M 1998 *Nature* **391** 62

[52] Collins P G, Zettl A, Bando H, Thess A and Smalley R E 1997 *Science* **278** 100

[53] Tans S J *et al* 1997 *Nature* **386** 474

[54] Bockrath M *et al* 1997 *Science* **275** 1922

[55] Dekker C 1999 *Phys. Today* **52** 22

[56] Yao Z, Kane C L and Dekker C 2000 *Phys. Rev. Lett.* **84** 2941

[57] Berber S, Kwon Y K and Tomanek D 2000 *Phys. Rev. Lett.* **84** 4613

[58] Bezryadin A, Verschueren A R M, Tans S J and Dekker C 1998 *Phys. Rev. Lett.* **80** 4036

[59] Rochefort A, Avouris P, Lesage F and Salahub D R 1998 *Chem. Phys. Lett.* **297** 45
     Rochefort A, Avouris P, Lesage F and Salahub D R 1999 *Phys. Rev.* B **60** 13 824

[60] Kılıç Ç, Ciraci S, Gulseren O and Yildirim T 2000 *Phys. Rev.* B **62** R16 345

[61] Angelescu D E, Cross M C and Roukes M L 1998 *Superlatt. Microstruct.* **23** 673

[62] Rego L G C and Kirczenow G 1988 *Phys. Rev. Lett.* **81** 232

[63] Buldum A, Ciraci S and Fong C Y 2000 *J. Phys.: Condens. Matter* **12** 3349

[64] Buldum A, Leitner D M and Ciraci S 1999 *Europhys. Lett.* **47** 208

[65] Özpineci A and Ciraci S 2001 *Phys. Rev.* B **63** 125415

[66] Sharvin Y V 1965 *Zh. Eksp. Teor. Fiz.* **48** 984 (Engl. Transl 1965 *Sov. Phys.–JETP* **21** 655)

[67] Sharvin Y V and Bogatina N I 1969 *Sov. Phys.–JETP* **29** 419

[68] Engquist H L and Anderson P W 1981 *Phys. Rev.* B **24** 1151

[69] Büttiker M, Imry Y, Landauer R and Pinhos S 1985 *Phys. Rev.* B **31** 6207

[70] Imry Y 1986 *Directions in Condensed Matter Physics* ed G Grinstein and G Mazenko (Singapore: World Scientific) p 101
[71] Imry Y 1997 *Mesoscopic Physics* (Oxford: Oxford University Press)
[72] Datta S 1995 *Electronic Transport in Mesoscopic Systems* (Cambridge: Cambridge University Press)
[73] Büttiker M 1986 *Phys. Rev. Lett.* **57** 1761
[74] Kirczenow G 1988 *Solid State Commun.* **68** 715
[75] Glazman L I, Lesovik G B, Khmelnitskii D E and Shekhter R I 1988 *Pis. Zh. Eksp. Teor. Fiz.* **48** 238
[76] Szafer A and Stone A D 1989 *Phys. Rev. Lett.* **60** 300
[77] Tekman E and Ciraci S 1989 *Phys. Rev.* B **39** R8772
[78] Escapa L and Garcia N 1989 *J. Phys.: Condens. Matter* **1** 2125
[79] Yacoby A and Imry Y 1990 *Phys. Rev.* B **41** 5341
[80] Kouwenhoven L P *et al* 1989 *Phys. Rev.* B **39** 8040
[81] Escapa L and Garcia N 1990 *Appl. Phys. Lett.* **56** 901
[82] Tekman E and Ciraci S 1989 *Phys. Rev.* B **42** R1860
[83] Kander I, Imry Y and Sivan U 1990 *Phys. Rev.* B **41** 12 941
[84] Tekman E and Ciraci S 1989 *Phys. Rev.* B **40** R8559
[85] Büttiker M 1990 *Phys. Rev.* B **41** 7906
[86] Chu C S and Sorbello R S 1989 *Phys. Rev.* B **40** 5941
[87] Masek J, Lipavsky P and Kramer B 1989 *J. Phys.: Condens. Matter* **1** 6395
[88] Tekman E and Ciraci S 1990 *Phys. Rev.* B **42** 9098
[89] Faist J, Guéret P and Rothuizen H 1990 *Phys. Rev.* B **42** 3217
[90] Smith C G *et al* 1988 *J. Phys. C: Solid State Phys.* **21** L893
[91] McEuen P L, Alpenhaar B W, Wheeler R G and Sacks R N 1990 *Surf. Sci.* **229** 312
[92] Bogachek E N, Zagoskin A M and Kulik I O 1990 *Fiz. Nizk. Temp.* **16** 1404 (Engl. Transl. 1990 *Sov J. Low Temp. Phys.* **16** 796)
[93] Economou E N and Soukoulis C M 1981 *Phys. Rev. Lett.* **46** 618
[94] Choi H C and Ihm J 1999 *Phys. Rev.* B **59** 2267
     Choi H C and Ihm J 1999 *Solid State Commun.* **111** 385
[95] Hirose K and Tsukada M 1995 *Phys. Rev.* B **51** 5278
[96] Nardelli M B 1999 *Phys. Rev.* B **60** 7828
[97] Chico L, Benedict L X, Louie S G and Cohen M L 1996 *Phys. Rev.* B **54** 2600
[98] Garcia-Moliner F and Velasco V R 1991 *Phys. Rep.* **200** 83
[99] Anantram M P and Govindan T R 1998 *Phys. Rev.* B **58** 4882
[100] Sutton A P and Pethica J B 1990 *J. Phys.: Condens. Matter* **2** 5317
[101] Landman U, Luedtke W D, Burnham N A and Colton R J 1990 *Science* **248** 454
[102] Portal D S, Artacho E, Junquera J, Ordejon P, Garcia A and Soler J M 1999 *Phys. Rev. Lett.* **83** 3884
[103] Häkkienen H *et al* 1999 *J. Phys. Chem.* B **103** 8814
[104] Gulseren O, Ercolesi F and Tosatti E 1998 *Phys. Rev. Lett.* **80** 3775
[105] Kondo Y and Takayanagi K 2000 *Science* **289** 600
[106] Tosatti E and Prestipino S 2000 *Science* **289** 561
     Tosatti E *et al* 2001 *Science* **291** 288
[107] Barnett R N and Landman U 1997 *Nature* **387** 788
[108] Thouless D J and Kirkpatrick S 1981 *J. Phys. C: Solid State Phys.* **14** 235
[109] Imry Y and Shiren N S 1986 *Phys. Rev.* B **33** 7992
[110] Ciraci S and Batra I P 1986 *Phys. Rev.* B **33** 4294
[111] Batra I P, Ciraci S, Srivastava G P, Nelson J S and Fong C Y 1986 *Phys. Rev.* B **34** 8246
[112] Ekardt W 1984 *Phys. Rev.* B **29** 1558
[113] Stafford C A, Baeriswyl D and Burki J 1997 *Phys. Rev. Lett.* **79** 2863
[114] Scheer E *et al* 1998 *Nature* **394** 154
[115] Kalmeyer V R and Laughlin R B 1987 *Phys. Rev.* B **35** 9805
[116] Bethune D S *et al* 1993 *Nature* **363** 605
[117] Thess A *et al* 1996 *Science* **273** 483
[118] Saito R, Fujita M, Dresselhaus G and Dresselhaus M S 1992 *Appl. Phys. Lett.* **60** 2204
[119] Mintmire J W, Dunlap B I and White C T 1992 *Phys. Rev. Lett.* **68** 631
[120] Hamada N, Sawada S and Oshiyama O 1992 *Phys. Rev. Lett.* **68** 1579
[121] Blase X, Benedict L X, Shirley E L and Louie S G 1994 *Phys. Rev. Lett.* **72** 1848
[122] White C T, Robertson D and Mintmire J W 1993 *Phys. Rev.* B **47** 5385
[123] Park C J *et al* 1999 *Phys. Rev.* B **60** 10 656

Yang L *et al* 1999 *Phys. Rev.* B **60** 13874

[124] Kilic C, Ciraci S, Gulseren O and Yildirim T 2000 *Phys. Rev.* B **62** R16345

[125] Langer L *et al* 1994 *J. Mater. Res.* **9** 927

[126] Dai H, Wong E W and Lieber C B 1996 *Science* **272** 523

[127] Ebbesen T W *et al* 1996 *Nature* **382** 54

[128] Nygard J, Cobden D H, Bockrath M, McEuen P L and Lindelof P E 1999 *Appl. Phys.* A **69** 297

[129] Soh H *et al* 1999 *Appl. Phys. Lett.* **75** 627

[130] Zhou C, Kong J and Dai H 2000 *Phys. Rev. Lett.* **84** 5604

[131] Tomanaga S I 1950 *Prog. Theor. Phys.* **5** 54
     Luttinger J M 1963 *J. Math. Phys.* **15** 609

[132] Kane C, Balents L and Fisher M P A 1997 *Phys. Rev. Lett.* **79** 5086

[133] Egger R and Gogolin A O 1997 *Phys. Rev. Lett.* **79** 5082

[134] Bockrath M *et al* 1999 *Nature* **397** 598

[135] Frank S, Poncharal P, Wang Z L and de Heer W A 1998 *Science* **280** 1744

[136] Tian W and Datta S 1994 *Phys. Rev.* B **49** 5097

[137] Saito R, Dresselhaus G and Dresselhaus M S 1996 *Phys. Rev.* B **53** 2044

[138] Tamura R and Tsukada M 1997 *Phys. Rev.* B **55** 4991

[139] Sanvito S, Kwon Y K, Tomanek D and Lambert C J 2000 *Phys. Rev. Lett.* **84** 1974

[140] Tans S J, Verschueren A R M and Dekker C 1998 *Nature* **393** 49

[141] Chico L, Crespi V H, Benedict L X, Louie S G and Cohen M L 1996 *Phys. Rev. Lett.* **76** 971

[142] Lambin Ph, Fonseca A, Vigneron J P, Nagy J B and Lucas A A 1995 *Chem. Phys. Lett.* **245** 85

[143] Han J, Anantram M P, Jaffe R L, Kong J and Dai H 1998 *Phys. Rev.* B **57** 14 983

[144] Amelinckx S *et al* 1994 *Nature* **265** 635

[145] Zhang X F and Zhang Z 1995 *Phys. Rev.* B **52** 5313
     Zhou D and Seraphin S 1995 *Chem. Phys. Lett.* **238** 286

[146] Yao Z, Postma H W Ch, Balents L and Dekker C 1999 *Nature* **402** 273

[147] Hu J, Ouyang M, Yang P and Lieber C B 1999 *Nature* **399** 48

[148] Papadopoulos C, Rakitin A, Li J, Vedeneev A S and Xu J M 2000 *Phys. Rev. Lett.* **85** 3476

[149] Buldum A and Lu J P 2001 *Phys. Rev.* B **63** R161403

[150] Fuhrer M S *et al* 2000 *Science* **288** 494

[151] Paulson S *et al* 2001 *Science* **280** 1742

[152] Falvo M R, Taylor R M, Helser A, Chi V, Brooks F P, Washburn S and Superfine R 1999 *Nature* **397** 236

[153] Buldum A and Lu J P 1999 *Phys. Rev. Lett.* **83** 5050

[154] Rueckes T *et al* 2000 *Science* **289** 94

[155] Batra I P and Ciraci S 2001 to be published

[156] Proetto C 1989 *Solid State Commun.* **80** 909
     Greiner A, Reggiani L, Kuhn T and Varani L 1996 *Phys. Rev. Lett.* **78** 1114

[157] Streda P 1989 *J. Phys.: Condens. Matter* **1** 1025

[158] Bogachek E, Scherbakov A G and Landman U 1999 *Phys. Rev.* B **60** 11 678

[159] Keldysh L V 1965 *Sov. Phys.–JETP* **20** 1018

[160] Pastawski H M 1992 *Phys. Rev.* B **46** 4053